NOV 9 1964

5

Copy No. 10

NASA General Working Paper No. 10,041

USE OF PARAMETRIC EQUATIONS TO OPTIMIZE A LANDING ROCKET AND SUBSEQUENT MODEL TESTING

[redacted]

[redacted]

SEP 1970
RECEIVED
NASA STI FACILITY
INPUT BRANCH

NATIONAL AERONAUTICS AND SPACE ADMINISTRATION
MANNED SPACECRAFT CENTER
Houston, Texas

October 21, 1964

N70-75388
(ACCESSION NUMBER) (THRU)
59 None
(PAGES) (CODE)
TMX 65052
(NASA CR OR TMX OR AD NUMBER) (CATEGORY)
FACILITY FORM 602

NASA GENERAL WORKING PAPER NO. 10,041

USE OF PARAMETRIC EQUATIONS TO OPTIMIZE A LANDING ROCKET AND SUBSEQUENT MODEL TESTING

Prepared by: Lonnie W. Jenkins

Lonnie W. Jenkins, AST
Auxiliary Propulsion and Pyrotechnics Branch

Chester A. Vaughan

Chester A. Vaughan, AST
Auxiliary Propulsion and Pyrotechnics Branch

James W. Akkerman

James W. Akkerman, AST
Auxiliary Propulsion and Pyrotechnics Branch

Authorized for Distribution:

Warren Gillespie, Jr.
for Maxime A. Faget
Assistant Director for Engineering and Development

NATIONAL AERONAUTICS AND SPACE ADMINISTRATION

MANNED SPACECRAFT CENTER

HOUSTON, TEXAS

October 21, 1964

TABLE OF CONTENTS

Page

SUMMARY 1

INTRODUCTION 1

SYMBOLS 2

DERIVATION OF MOTION RELATIONSHIPS 4

APPLICATION 8

SUSTAIN PHASE 11

CONCLUDING REMARKS 13

APPENDIX – PROPULSION MODEL DESCRIPTION AND TESTING 41

TABLE A-I – TIME AND PRESSURE RELATIONSHIPS OBTAINED DURING SYSTEM CHARACTERIZATION 44

TABLE A-II – CALCULATION METHOD FOR SEQUENCER SETTINGS OF COLD GAS SYSTEM 45

LIST OF FIGURES

Figure		Page
1	Dimensionless performance-boost phase	15
2	Dimensionless performance-sustain phase, $\nu_1 = 0.00$	17
3	Dimensionless performance-sustain phase, $\nu_1 = 0.05$	19
4	Dimensionless performance-sustain phase, $\nu_1 = 0.10$	21
5	Dimensionless performance-sustain phase, $\nu_1 = 0.15$	23
6	Dimensionless performance-sustain phase, $\nu_1 = 0.20$	25
7	Dimensionless performance-sustain phase, $\nu_1 = 0.25$	27
8	Dimensionless performance-sustain phase, $\nu_1 = 0.30$	29
9	Dimensionless performance-sustain phase, $\nu_1 = 0.35$	31
10	Dimensionless performance-sustain phase, $\nu_1 = 0.40$	33
11	Dimensionless performance-sustain phase, $\nu_1 = 0.45$	35
12	Dimensionless performance-sustain phase, $\nu_1 = 0.50$	37
13	Use of boost phase parametric charts	39

Figure Page

14 Use of sustain-phase parametric charts 39

15 Illustration of iteration scheme 40

A-1 Schematic of propulsion system (third-scale Gemini) . . . 46

A-2 Thrust stand used to calibrate cold gas propulsion system 47

A-3 Cold gas system thrust-chamber pressure calibration curve 48

A-4 Overall view of model propulsion system 49

A-5 Actuation time relationships for cold-gas propulsion system 50

A-6 Dome pressure-manifold pressure calibration curve 51

A-7 Dome pressure ratio as a function of valve open time. . . 52

A-8 Overall model test set-up 53

A-9 Typical cold gas thrust-time variation (drop 25) 54

A-10 Typical vertical acceleration, velocity, distance, and time relationships 55

USE OF PARAMETRIC EQUATIONS TO OPTIMIZE A LANDING ROCKET AND SUBSEQUENT MODEL TESTING

Lonnie W. Jenkins, Chester A. Vaughan
James W. Akkerman

SUMMARY

Parametric equations of motion for a retrorocket used in conjunction with a parachute for landing a spacecraft are derived. Their use in optimizing solid propellant rockets for a Gemini weight vehicle are discussed. A two-level thrust-time relationship is found necessary because of variations in vehicle velocity and rocket and altitude sensor performance. The development and use of a pressurized gas propulsion system for subscale testing is described.

INTRODUCTION

The use of parachutes for recovering a manned spacecraft after reentry was shown to be very reliable in the Mercury program. Due to the magnitude of the impact loads, all Mercury spacecraft landings were made in water. The achievement of land landings has become an objective of subsequent manned space programs. This goal requires an impact attenuation system to reduce both the magnitude and the onset rate of deceleration or g-loading. In order to keep the weight of such a system as light as possible, it is necessary to consider one having maximum energy absorption capability for a given weight. A good example is a solid propellant rocket motor. In addition, it is simple, compact, and can be stored for extended periods of time without performance degradation. The solid propellant rocket motor, in conjunction with an altitude sensing device, can be ignited at a preset distance above the ground, thus decreasing the descent rate of the vehicle from the parachute's relatively high terminal velocity to an allowable velocity at impact.

This paper derives parametric equations of motion and describes their use in optimizing a solid propellant landing rocket for use in conjunction with the Para-Sail parachute. These components comprise the basis for a backup program for Gemini land landings being directed by the Landing Technology Branch, Structures and Mechanics Division, and supported in the analysis and development of the landing rockets by the Auxiliary Propulsion and Pyrotechnic Branch of the Propulsion and Power Division.

SYMBOLS

F	Rocket thrust, lb
H	Thrust-to-weight ratio, boost phase
L	Thrust-to-weight ratio, sustain phase
P_1	High value of dome pressure, psig
P_2	High value of nozzle manifold pressure, psig
P_3	Low value of nozzle manifold pressure, psig
P_4	Low value of dome pressure, psig
T	Temperature, °F
V	Velocity, ft/sec
W	Weight, lb
d_D	Time delay from sequencer triggering to signal to open dome vent valve, msec
d_N	Time delay from sequencer triggering to signal to open the nozzle solenoid valve, msec
g	Acceleration due to gravity, 32.2 ft/sec^2
l	Length, ft
m	Mass $\left(\frac{W}{g}\right)$, slugs
t	Time, sec
t_D	Total time from sequencer triggering to signal to close the dome vent valve, msec
t_f	Free-fall duration to 90 percent of high pressure, msec
t_H	Boost phase duration, msec
t_N	Total time from sequencer triggering to signal to close the nozzle solenoid valve, msec
t_T	Total nozzle manifold pressure duration, msec

x	Distance traveled, ft
β	Drag force proportionality constant
Δt_A	Time from beginning of free-fall to sequence triggering, msec
Δt_1	Interval that dome vent valve is open $\left(t_D - d_D\right)$, msec
Δt_5	Time from opening of nozzle solenoid valve to 90 percent of maximum nozzle manifold pressure, msec
Δt_6	Time from closing of nozzle solenoid valve to beginning of decay of sustain phase nozzle manifold pressure, msec
Δt_{11}	Time from opening of dome vent valve to beginning of decay of boost phase nozzle manifold pressure, msec
λ	Constant
ν	Reduced velocity ratio, $\frac{V}{Vo}$
π_k	Temperature sensitivity of burning rate, $^{o}F^{-1}$
τ	Reduced time, $\frac{tg}{V_o}$
χ	Reduced distance traveled, $\frac{xg}{V_o^2}$

Subscripts:

o	Initial value
1	Value at end of boost phase
2	Value at end of sustain phase
A	Conditions pertaining to case A
B	Conditions pertaining to case B
H	Horizontal
i	Initial
f	final

im	Impact
del	Delay
nom	Nominal
V	Vertical

DERIVATION OF MOTION RELATIONSHIPS

In analyzing the motion of a spacecraft acted upon by the combined forces of gravity, parachute drag, and retrorockets, certain simplifying assumptions may be made:

a. The drag coefficient of the parachute is constant.

b. The drag force is proportional to the vertical velocity squared.

c. The vehicle is considered a rigid, point mass.

d. All forces are colinear.

e. There is no stretch in the parachute shroud lines.

f. There is no cross coupling between the horizontal and vertical forces.

g. The change of mass due to propellant loss is negligible.

The equations of motion may now be derived as follows:

Drag force = βV^2

Weight = W

Thrust = F(t)

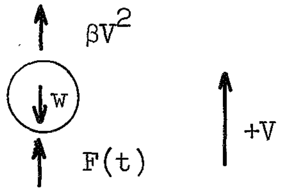

Summing the forces and using Newton's second law

$$\Sigma F = m \frac{dV}{dt} \qquad (1)$$

$$F(t) + \beta V^2 - W = \frac{W}{g} \frac{dV}{dt} \qquad (2)$$

Rearranging;

$$\frac{dV}{dt} = \frac{F(t)}{W} g + \beta \frac{gV^2}{W} - g \tag{3}$$

Prior to rocket ignition, the vehicle has reached a steady-state velocity, V_o, where the weight of the vehicle is equal to the drag force. The drag coefficient, therefore, can be determined by:

$$\beta V_o^2 = W \tag{4}$$

or

$$\beta = \frac{W}{V_o^2} \tag{5}$$

Equation (3) now becomes

$$dV = \left(\frac{F(t)}{W} + \frac{V^2}{V_o^2} - 1 \right) g\, dt \tag{6}$$

The solution to this differential equation is dependent on the variation of thrust with time and can be solved in closed form only when the thrust is constant. For a constant thrust-to-weight ratio (H) greater than one, the differential equation can be solved by separating the variables and direct integration.

Integration of equation (6) yields:

$$V_1 = V_o \sqrt{(H-1)} \tan \left(\frac{g}{V_o} \sqrt{(H-1)}\, t_1 + \tan^{-1} \left[\frac{1}{\sqrt{(H-1)}} \right] \right) \tag{7}$$

or rearranging,

$$\upsilon_1 = \sqrt{(H-1)} \tan \left(\tau_1 \sqrt{(H-1)} + \tan^{-1} \left[\frac{1}{\sqrt{(H-1)}} \right] \right) \tag{8}$$

where

$$\nu = \frac{V}{V_o} \qquad (9)$$

and

$$\tau = \frac{tg}{V_o} \qquad (10)$$

with the subscript "1" or "2" as applicable for V and t.

Integration of equation (7) yields:

$$x_1 = \frac{V_o^{\,2}}{g}\left(\ln\left\{\frac{\sqrt{(H-1)}}{\sqrt{(H-1)}\cos\left[\frac{gt_1}{V_o}\sqrt{(H-1)}\right] - \sin\left[\frac{gt_1}{V_o}\sqrt{(H-1)}\right]}\right\}\right) + x_o \qquad (11)$$

or rearranging,

$$\chi_1 = \ln\left(\frac{\sqrt{(H-1)}}{\sqrt{(H-1)}\cos\left[\tau_1\sqrt{(H-1)}\right] - \sin\left[\tau_1\sqrt{(H-1)}\right]}\right) \qquad (12)$$

where

$$\chi_1 = \frac{(x_1 - x_o)\,g}{V_o^{\,2}} \qquad (13)$$

Figure 1 shows a family of curves generated from equations (8) and (12). Reduced velocity, ν_1, is shown as a function of reduced distance traveled, χ_1, with the thrust-to-weight ratio, H, treated as a parameter. In addition, lines of constant reduced time, τ_1, are shown. Any two terms may be used to determine corresponding values of the other two terms. For example, the resulting reduced velocity and the distance may be obtained for a given combination of reduced time and thrust-to-weight ratio.

The above results apply for the boost phase ($H > 1$). It is further necessary to consider a sustain phase where the thrust-to-weight ratio, L, is less than one and constant. The initial conditions for this sustain phase are the end conditions for the boost phase.

Integration of equation (6) yields:

$$V_2 = V_o \sqrt{(1-L)} \; \frac{\left(1 + \lambda \, \mathrm{Exp}\left[\frac{2g \sqrt{(1-L)}}{V_o} t_2\right]\right)}{\left(1 - \lambda \, \mathrm{Exp}\left[\frac{2g \sqrt{(1-L)}}{V_o} t_2\right]\right)} \qquad (14)$$

where

$$\lambda = \frac{V_1 - V_o \sqrt{(1-L)}}{V_1 + V_o \sqrt{(1-L)}} \qquad (15)$$

This may be rearranged to

$$\nu_2 = \sqrt{(1-L)} \left(\frac{1 + \lambda \, \mathrm{Exp}\left[2\tau_2 \sqrt{(1-L)}\right]}{1 - \lambda \, \mathrm{Exp}\left[2\tau_2 \sqrt{(1-L)}\right]}\right) \qquad (16)$$

Integration of equation (14) yields

$$x_2 = V_o \sqrt{(1-L)} \, t_2 - \frac{V_o^{\,2}}{g} \ln\left(\frac{1 - \lambda \, \mathrm{Exp}\left[\frac{2g \sqrt{(1-L)}}{V_o} t_2\right]}{1 - \lambda}\right) + x_1 \qquad (17)$$

or, rearranging,

$$\chi_2 = \tau_2 \sqrt{(1-L)} - \ln\left(\frac{1 - \lambda \, \mathrm{Exp}\left[2\tau_2 \sqrt{(1-L)}\right]}{1 - \lambda}\right) \qquad (18)$$

where

$$\chi_2 = \frac{\left(x_2 - x_1\right)}{V_o^{\,2}} \, g \qquad (19)$$

Figures 2 through 12 each show a family of curves generated from equations (16) and (18) for values of reduced velocity at the end of boost phase, υ_1, ranging from 0 to 0.50. Reduced velocity, υ_2, is shown as a function of reduced distance traveled in the sustain phase, χ_2, with the sustain thrust-to-weight ratio, L, treated as a parameter. In addition, lines of constant reduced time, τ_2, are shown.

With the information presented in figures 1 through 12, and the assumptions mentioned, the rocket performance envelope can be determined for any system.

APPLICATION

In determining performance requirements of solid propellant rockets for the development program of the Para-Sail landing rocket system mentioned previously, it is necessary to consider variations, as well as the nominal values, of the systems' parameters. The magnitude and ranges of these, which were specified for the development program, were as follows:

a. Rate of descent: $V_o = 30 \pm 3$ ft/sec

b. Impact velocity: $V_{im} \leq 10$ ft/sec

c. Operating environment:

  (1) Nominal temperature: 70° F

  (2) Temperature limits: 40 to 140° F

  (3) Altitude: sea level

d. Altitude sensor actuation signal variation: ±5 percent of the nominal distance

e. Rocket ignition time variation: ±10 msec

f. Rocket performance variation: ±5 percent of the thrust at a given temperature

g. Vehicle weight: 4550 pounds

The nominal rate of descent listed is the terminal value of the proposed parachute. The maximum impact velocity given is approximately the design limitation of the present Gemini landing gear. The expected temperature environment for the proposed location of the rocket motors in the Gemini vehicle determined the operating temperature limit range. From various studies of altitude sensors, it is felt that, for actuation heights of 5 to 40 feet above the ground, a sensor can be chosen that will be accurate within ±5 percent. Using present technology for solid propellant rockets, the deviation in rocket ignition time of ±10 milliseconds and the ±5 percent variation on thrust level can be met without imposing undue hardships on the rocket manufacturer.

The variation of rocket performance with temperature is expressed by a temperature sensitivity coefficient $\left(\pi_k\right)$ which is dependent upon the particular propellant considered. For purposes of this analysis, the value of π_k is assumed to be 0.11 percent variation per degree Fahrenheit change in temperature. The calculation of thrust and burning time with temperature variations is based on the well established assumption that total impulse is constant. Thus:

$$F_f = F_i \operatorname{Exp}\left[\pi_k \left(T_f - T_i\right)/100\right] \tag{20}$$

$$t_f = t_i \operatorname{Exp}\left[\pi_k \left(T_i - T_f\right)/100\right] \tag{21}$$

$$F_B = 1.05\ F_{nom} \tag{22}$$

$$F_A = 0.95\ F_{nom} \tag{23}$$

In determining the changes in vehicle motion caused by performance variation, this report considers their effect in "worse-coupled" conditions. These are:

a. The combination of the highest predicted initial velocity coupled with the lowest predicted thrust (case A), and

b. The combination of the lowest predicted initial velocity coupled with the highest predicted thrust (case B).

In order to keep this system as simple as possible, altitude is the only parameter utilized to determine the proper time for igniting the rocket. Upon examining cases A and B discussed above, it is evident that case A results in a greater distance traveled during rocket firing than does case B. It is undesirable to impact with a net positive acceleration since this would result in a rebound with a second impact of unknown velocity and attitude. The altitude set for igniting the rocket must therefore be at least as great as the distance traveled in case A. This means that in case B, the rocket will burn out before impact, and the vehicle will free-fall the remaining distance. Depending upon the magnitude of the free-fall distance, the impact velocity may be excessive. For this event a second, lower, thrust level (sustain phase as opposed to the first or boost phase) with a thrust-to-weight ratio less than one is required to achieve the desired reduced velocity.

Case A - The minimum thrust occurs at +40° F, and the highest pre dicted initial velocity is 33 ft/sec with a maximum allowable impact velocity of 10 ft/sec. An upper limit of υ_{1A} can be established:

$$\upsilon_{1A} = \frac{10}{33} = 0.30$$

There must be some allowance for altitude sensor actuation and ignition delay time variances; however, this value will serve as a first approximation. After selecting a value of $H_A = 2.4$, τ_{1A} and χ_{1A} can be obtained from figure 1 with $\upsilon_{1A} = 0.30$ and $H_A = 2.4$. This results in $\tau_{1A} = 0.38$, and $\chi_{1A} = 0.238$; or $t_{1A} = 0.39$ sec, and $x_{1A} = 8.05$ ft. The use of figure 1 is better illustrated in figure 13.

Case B - The minimum predicted initial velocity is 27 fps, and the maximum thrust will occur at 140° F. Using equations (20) through (23):

$$H_B = \left(\frac{1.05}{0.95}\right) (2.4) \operatorname{Exp} \left[0.0011 \ (140 - 40)\right] = 2.96$$

$$t_{1B} = 0.39 \operatorname{Exp} \left[0.0011 \ (40 - 140)\right] = 0.35$$

The corresponding value of τ_{1B} is 0.42. From figure 1, $\upsilon_{1B} = 0.06$ and $\chi_{1B} = 0.204$, or $V_{1B} = 1.62$ ft/sec and $x_{1B} = 4.64$ ft.

For case B the vehicle has to travel 3.41 feet after the end of boost thrust. If the vehicle were allowed to free-fall for this distance, with an initial free-fall velocity of 1.62 ft/sec, the velocity at impact would be 14.9 ft/sec. This being greater than the maximum allowable impact velocity, a sustain-thrust phase is required.

SUSTAIN PHASE

The most efficient sustain phase thrust-to-weight ratio (L) allows an impact velocity of 10 ft/sec when the total distance traveled for both the boost and sustain phase in case B is equal to the distance traveled for the boost phase in case A.

The vehicle has to travel through a distance of 3.41 ft $\left(\chi_{2B} = 0.150\right)$ during the sustain phase for case B. Values of L_B and τ_{2B} can be obtained by interpolation between figures 3 and 4 using $\upsilon_{1B} = 0.06$, $\chi_{2B} = 0.150$, and $\upsilon_{2B} = 0.37$. The results obtained are $L_B = 0.48$ and $\tau_{2B} = 0.68$. The use of figure 3 is better illustrated in figure 14.

It is now necessary to include the effects of altitude sensor and ignition delay time variations. The ignition delay variation may be converted to a distance variation by multiplying it by the maximum initial velocity:

$$x_{del} = (0.010)\ (33) = 0.33 \text{ ft.}$$

Thus the nominal altitude sensor setting would be:

$$x_{nom} = 8.05 + 0.33 + 0.05\ x_{nom}$$

or

$$x_{nom} = 8.82 \text{ ft}$$

This value means that the vehicle must travel 0.77 ft in case A during the sustain phase $\left(\chi_{2A} = 0.023\right)$. The corresponding reduced velocity, υ_{2A}, is obtained from figure 8 with $\upsilon_{1A} = 0.30$ and $L_A = 0.39$, giving a value of $\upsilon_{2A} = 0.34$ or $V_{2A} = 11.1$ ft/sec. A lower value of impact velocity is required.

Either the burning time and/or the value of H must be decreased. The limit to these changes is the combination which would make the value ν_{1B} equal to zero. From figure 1, keeping $H_B = 2.96$, a value of $\tau_{1B} = 0.44$ will result in $\nu_{1B} = 0$. A first approximation for a new value of τ_{1B} is $\tau_{1B} = \left(\tau_{1B} + 0.44\right) 0.5 = (0.42 + 0.44)\ 0.5 = 0.43$, which is equivalent to $t_{1B} = 0.36$ sec or $t_{1A} = 0.40$ sec. A second pass through the calculation scheme outlined gives the following values: $H_A = 2.4$, $x_{nom} = 8.96$ ft, $\tau_{1A} = 0.39$, $L_A = 0.46$, and $V_{2A} = 10.6$ ft/sec.

The two values for τ_{1B} thus far used, and the resulting values of V_{2A}, are shown in figure 15. This suggests that a value of V_{2A} less than 10.0 ft/sec will not be attained with the set of values chosen and the restraints imposed. Indeed, using the limiting value of $\tau_{1B} = 0.44$, a value of $V_{2A} = 10.3$ ft/sec ensues. This analysis has been based on a constant thrust with time in both the boost and sustain phase. It also assumes that the transition between the boost and sustain phase is instantaneous. Obviously, from an internal ballistics standpoint, the thrust will probably not be constant with time. Also, the transition from boost to sustain phase will require a finite amount of time. The result of these factors will, in general, be in a direction which increases the deceleration of the capsule.

Although the ramp function described is a good representation of the required performance, the actual thrust-time relationship should be used in equation (5) when it becomes available.

In summary, the nominal (70°) performance parameters of the landing rockets are as follows: $t_1 = 0.40$ sec, $t_2 = 0.89$ sec, $H = 2.61$, $L = 0.50$, and $x_{nom} = 9.0$ ft.

In the prototype vehicle selected for the Para-Sail landing rocket program, the rockets are revolved 8° about the roll axis in opposing directions. This reduces the vertical component of thrust by the cosine of 8°. These factors may be combined to give the following required performance for each of the landing rockets for the Para-Sail landing rocket system:

	Boost	Sustain
Thrust, lb_f	6,000	1,150
Burning time, sec	0.40	0.89

Thiokol Chemical Corporation (Elkton) has been selected to manufacture solid propellant rockets having these thrust-time requirements for the above-mentioned program. The appendix describes a cold gas propulsion system which was built for use in a subscale model.

CONCLUDING REMARKS

The thrust-time variation of a solid propellant rocket used to provide impact attenuation for a vehicle descending to earth by means of a parachute may be designed to provide for many performance variations. These include variations in propellant burning rate and temperature, rate of descent, altitude sensor actuation signal, and ignition delay time. For those systems where the variations are large, a second, lower thrust level must be provided.

The method is applicable for all parachute-landing rocket systems where the net force of the rocket(s) acts vertically through the c.g. This includes a proposed military usage for palletized cargo.

NASA-S-64-6310

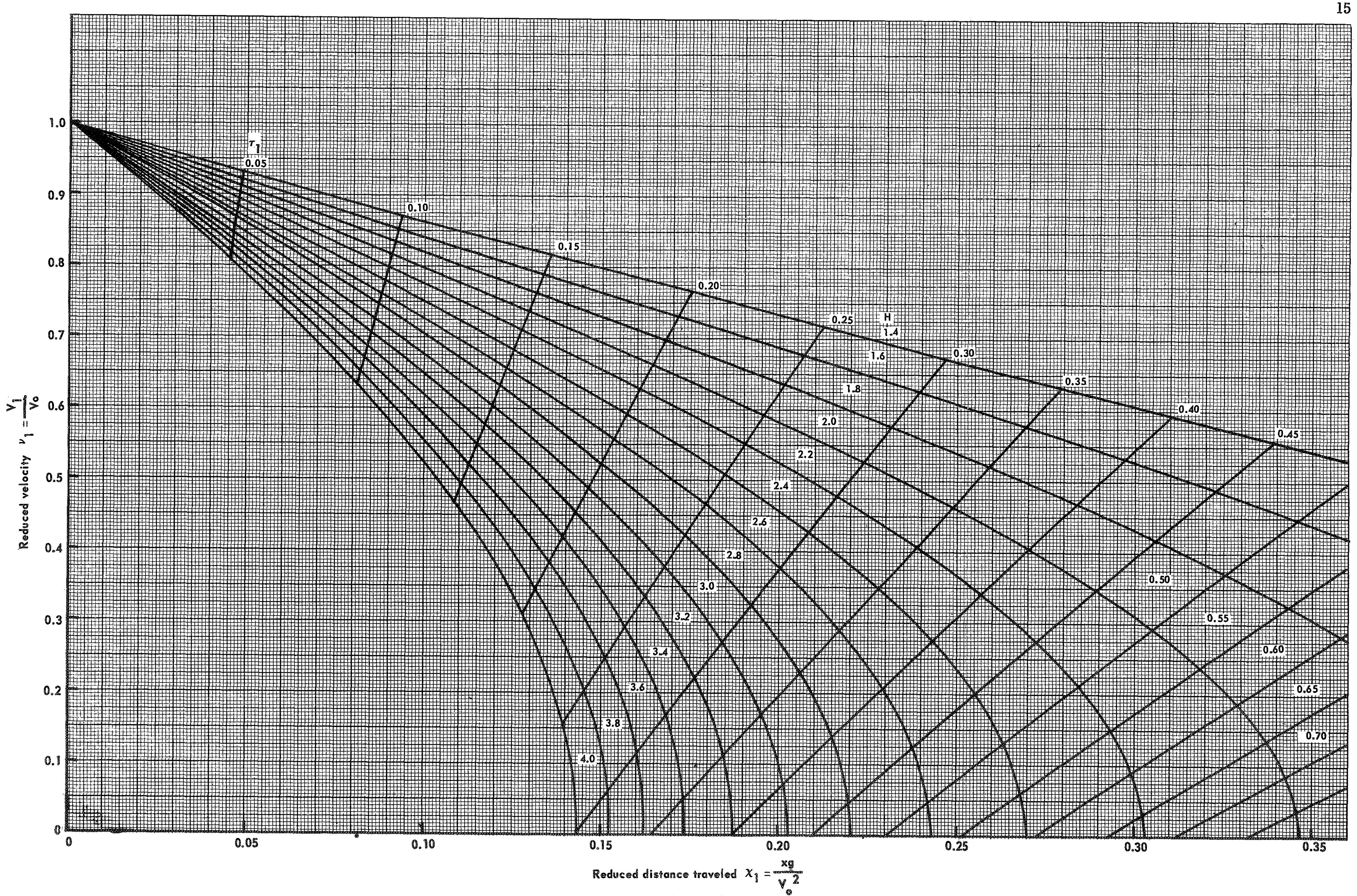

Figure 1 - Dimensionless performance - boost phase

NASA-S-64-6311

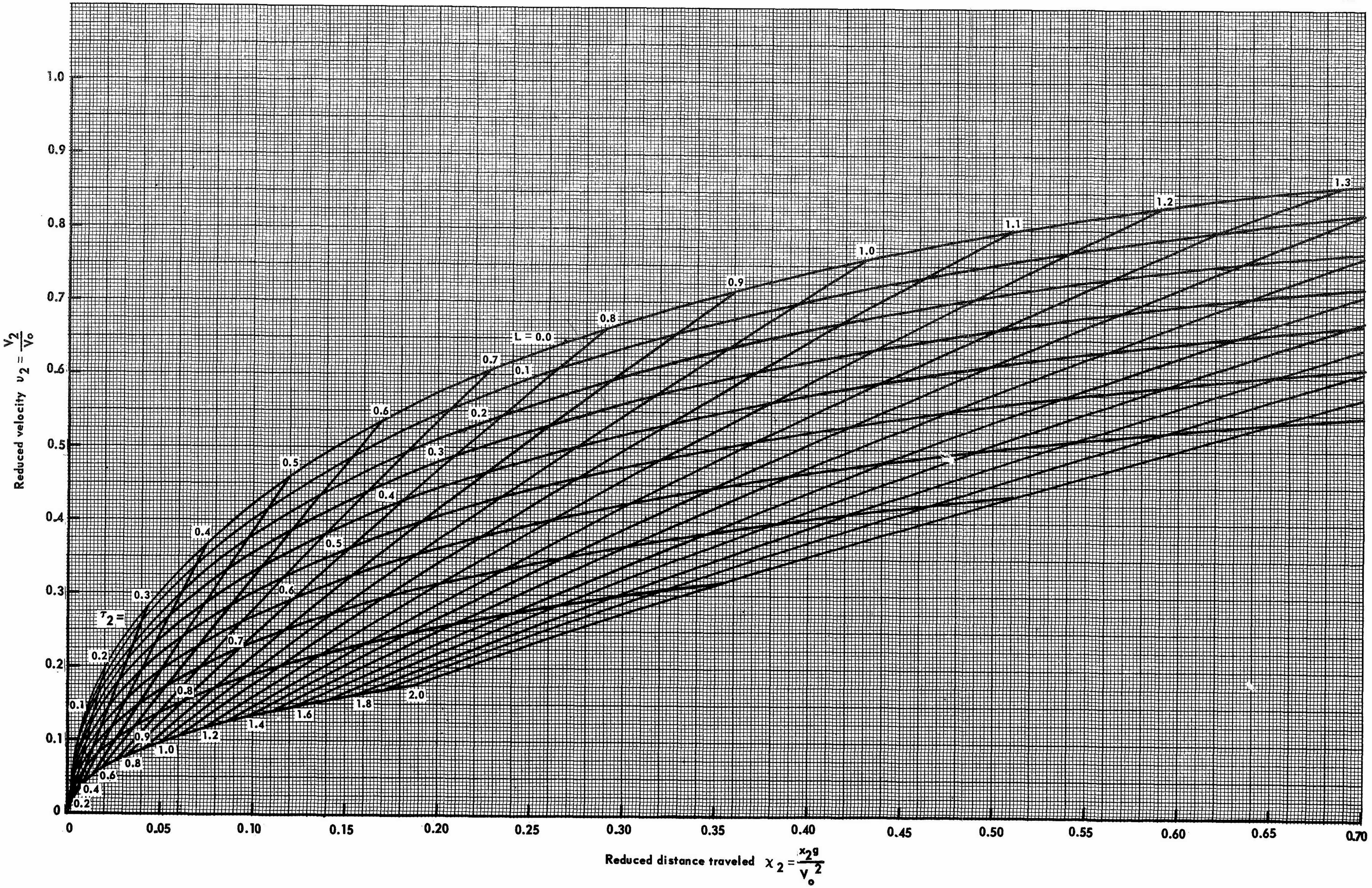

Figure 2 - Dimensionless performance - sustain phase $\nu_1 = 0.00$

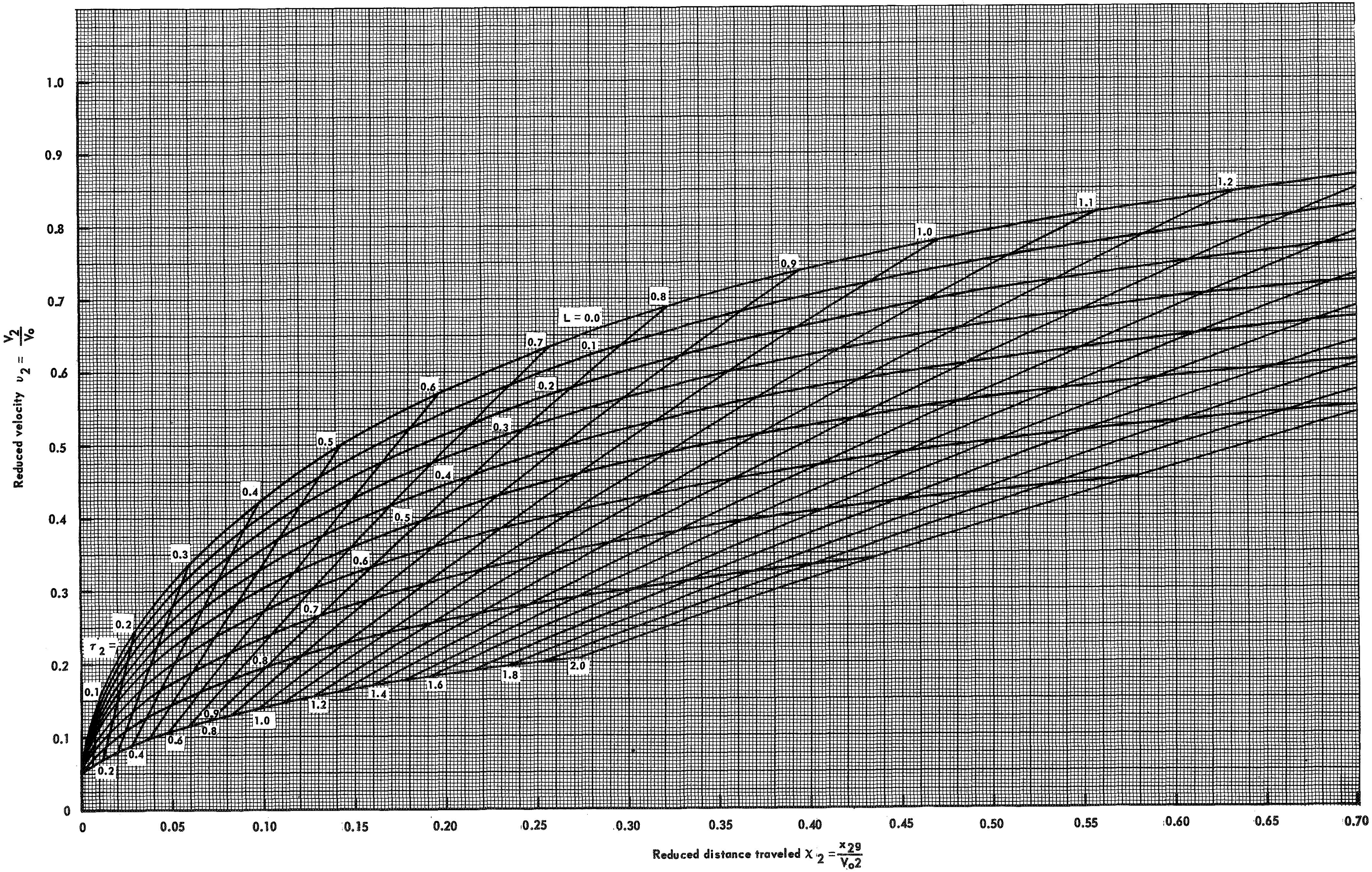

Figure 3 - Dimensionless performance - sustain phase $\nu_1 = 0.05$

NASA-S-64-6313

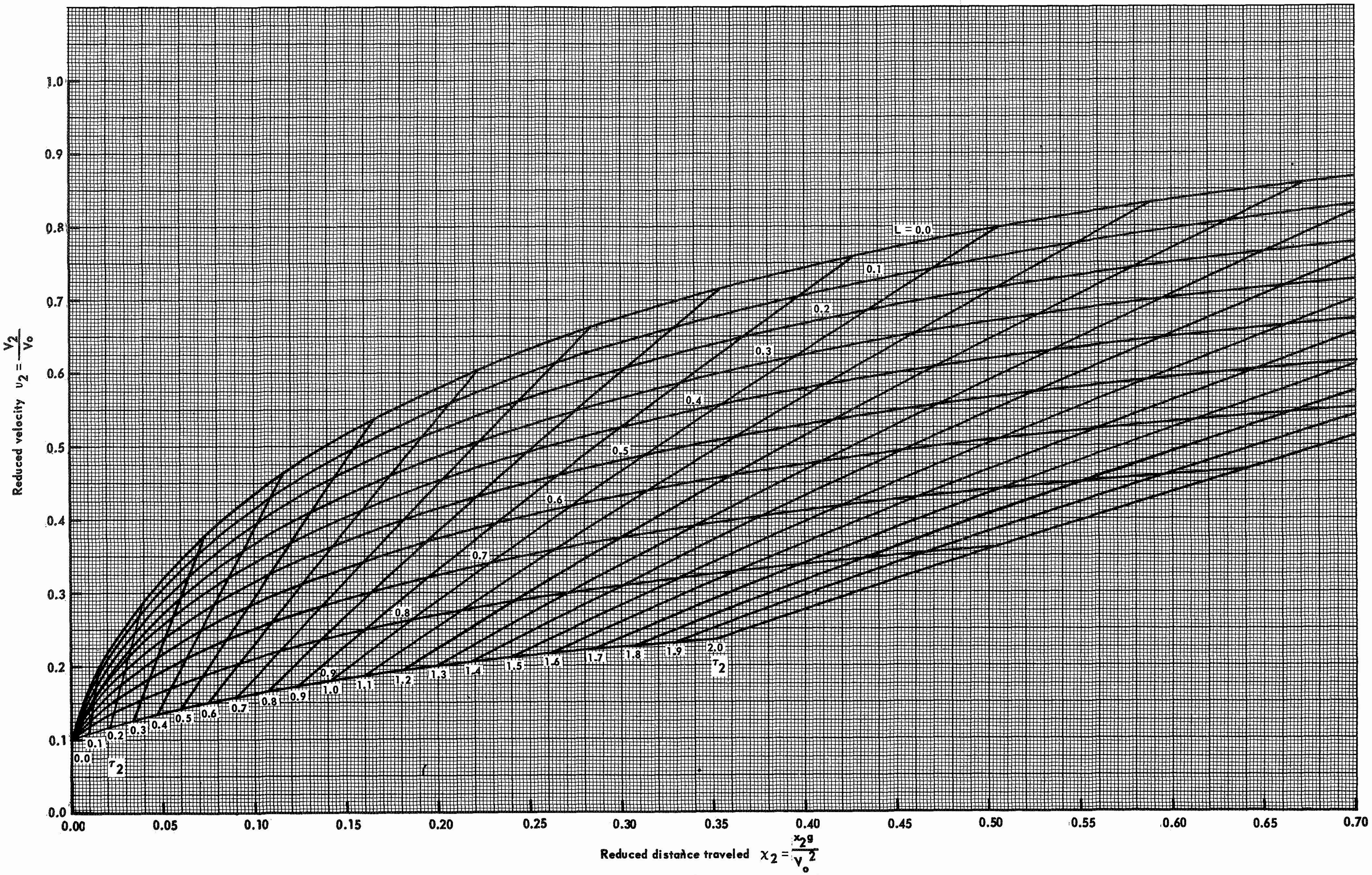

Figure 4 - Dimensionless performance - sustain phase $\upsilon_1 = 0.10$

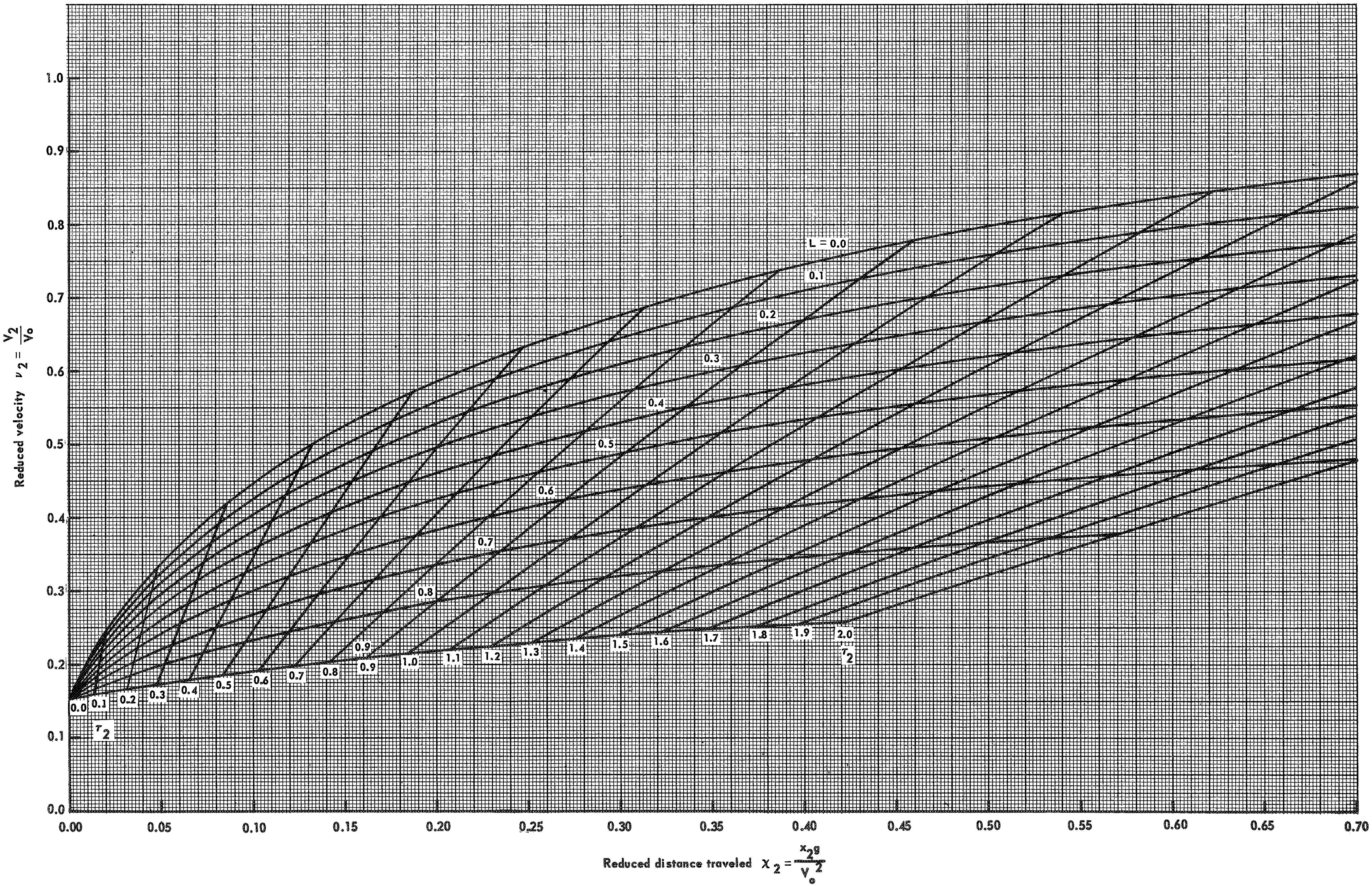

Figure 5 - Dimensionless performance - sustain phase $\nu_1 = 0.15$

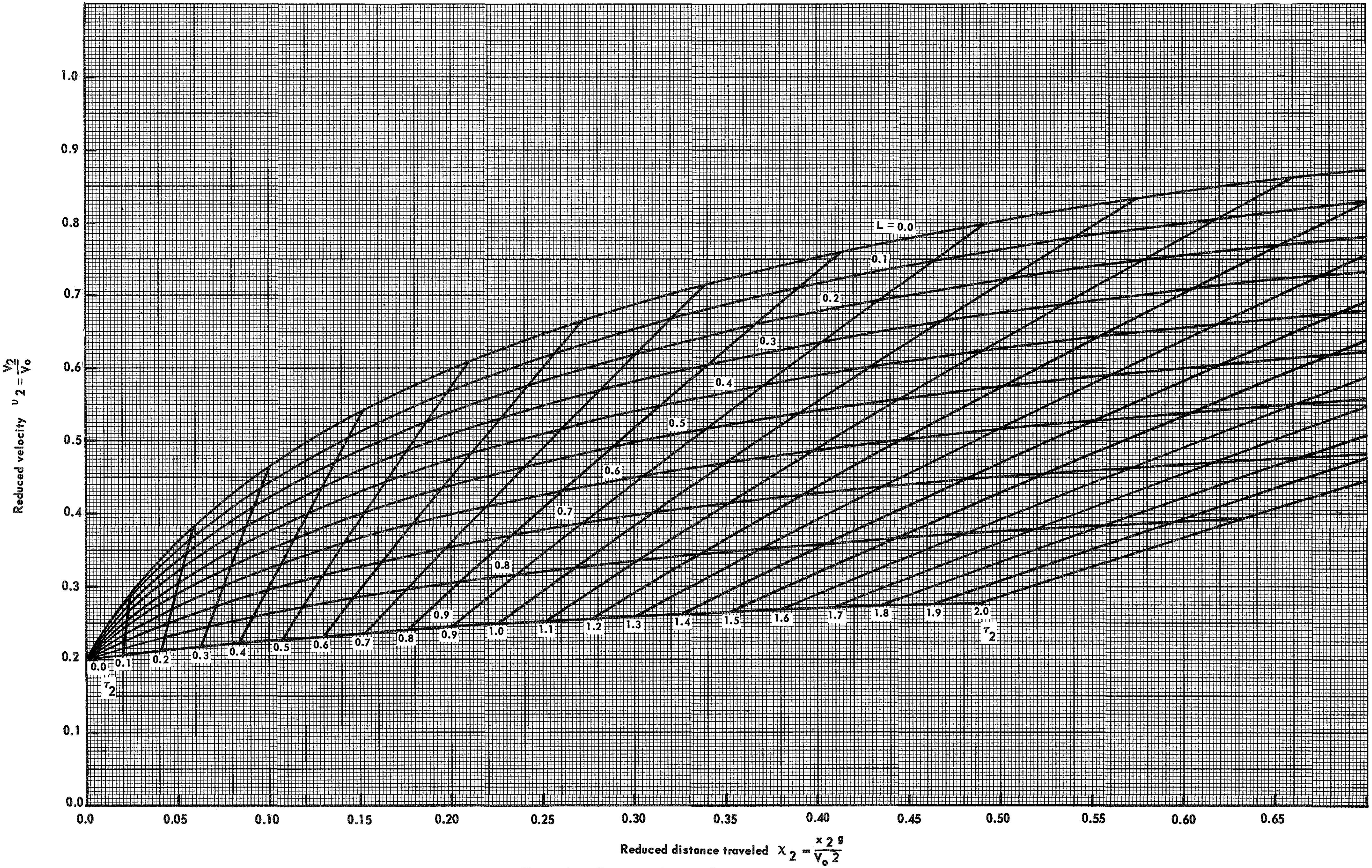

Figure 6 - Dimensionless performance - sustain phase $\nu_1 = 0.20$

NASA-S-64-6316

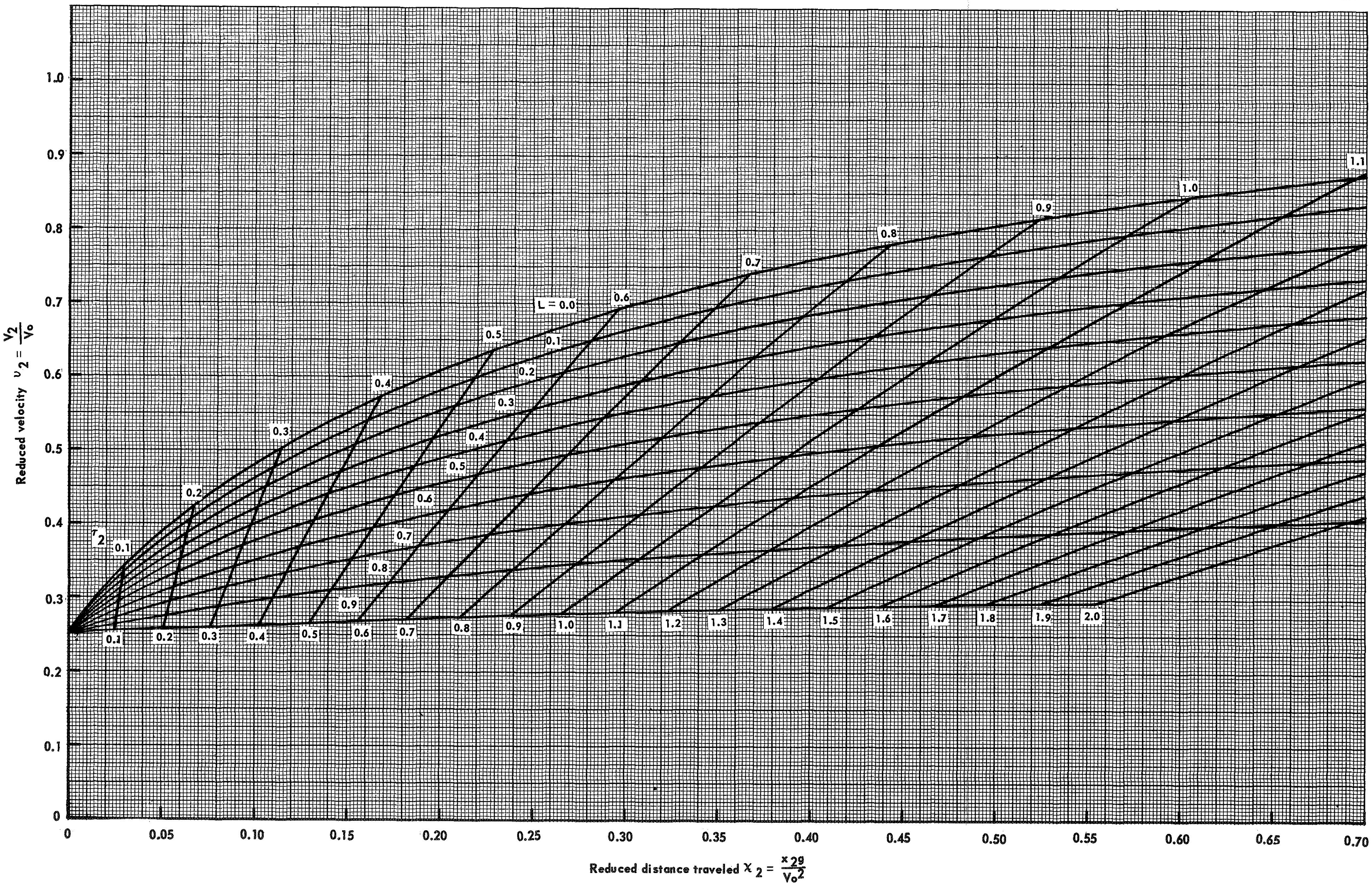

Figure 7 - Dimensionless performance - sustain phase $\nu_1 = 0.25$

NASA-S-64-6317

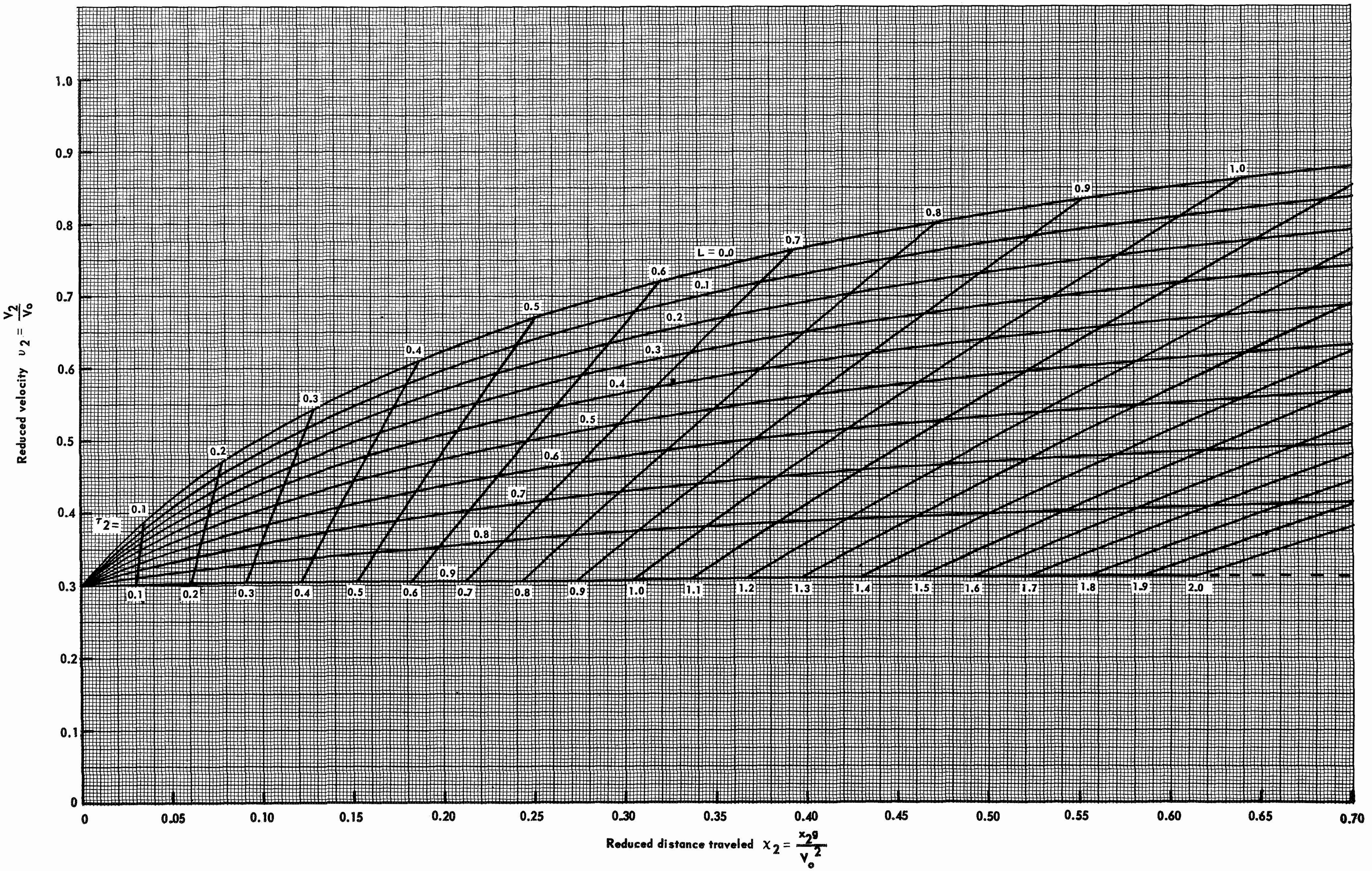

Figure 8 - Dimensionless performance - sustain phase $\upsilon_1 = 0.30$

NASA-S-64-6318

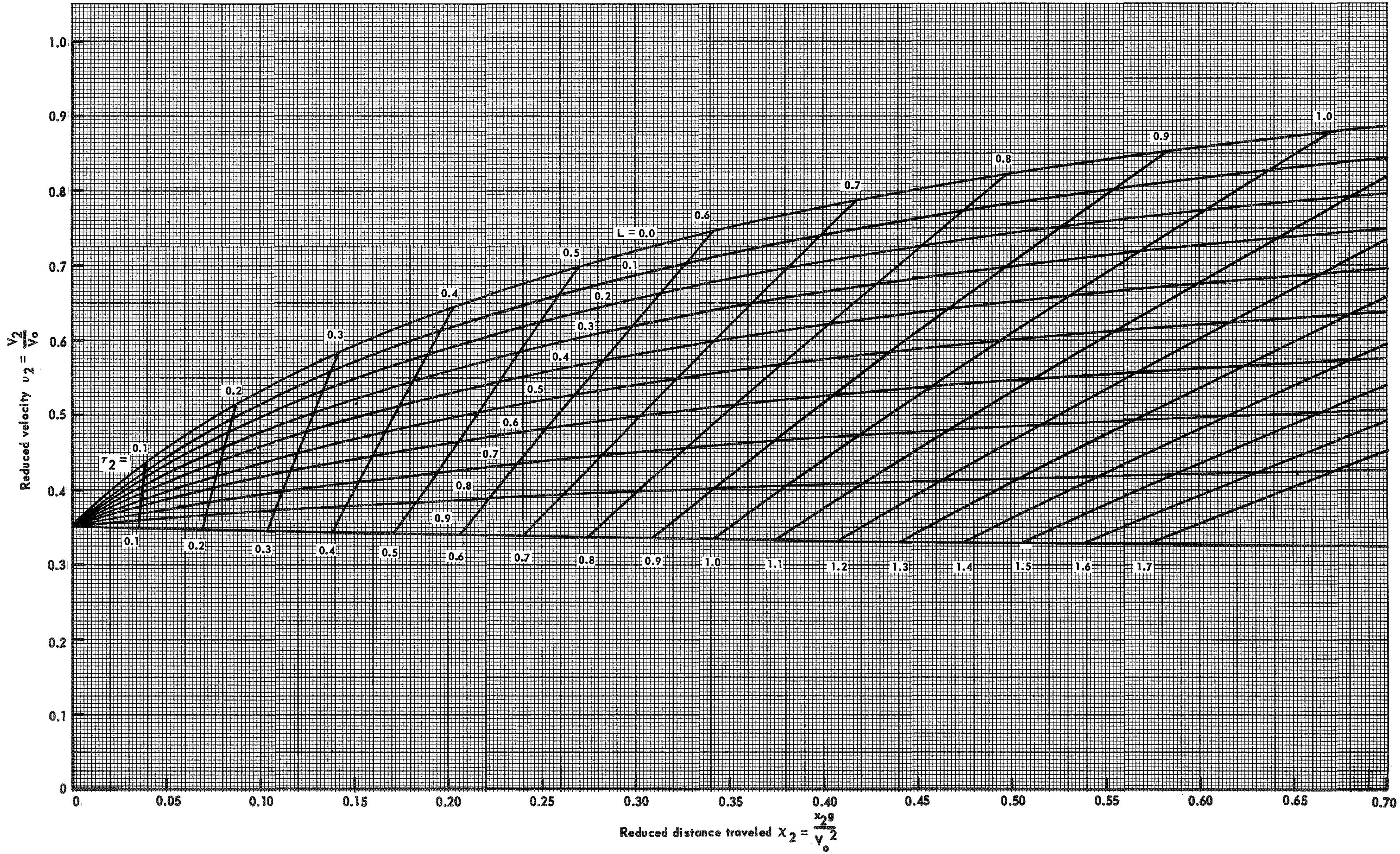

Figure 9 - Dimensionless performance - sustain phase $\upsilon_1 = 0.35$

NASA-S-64-6319

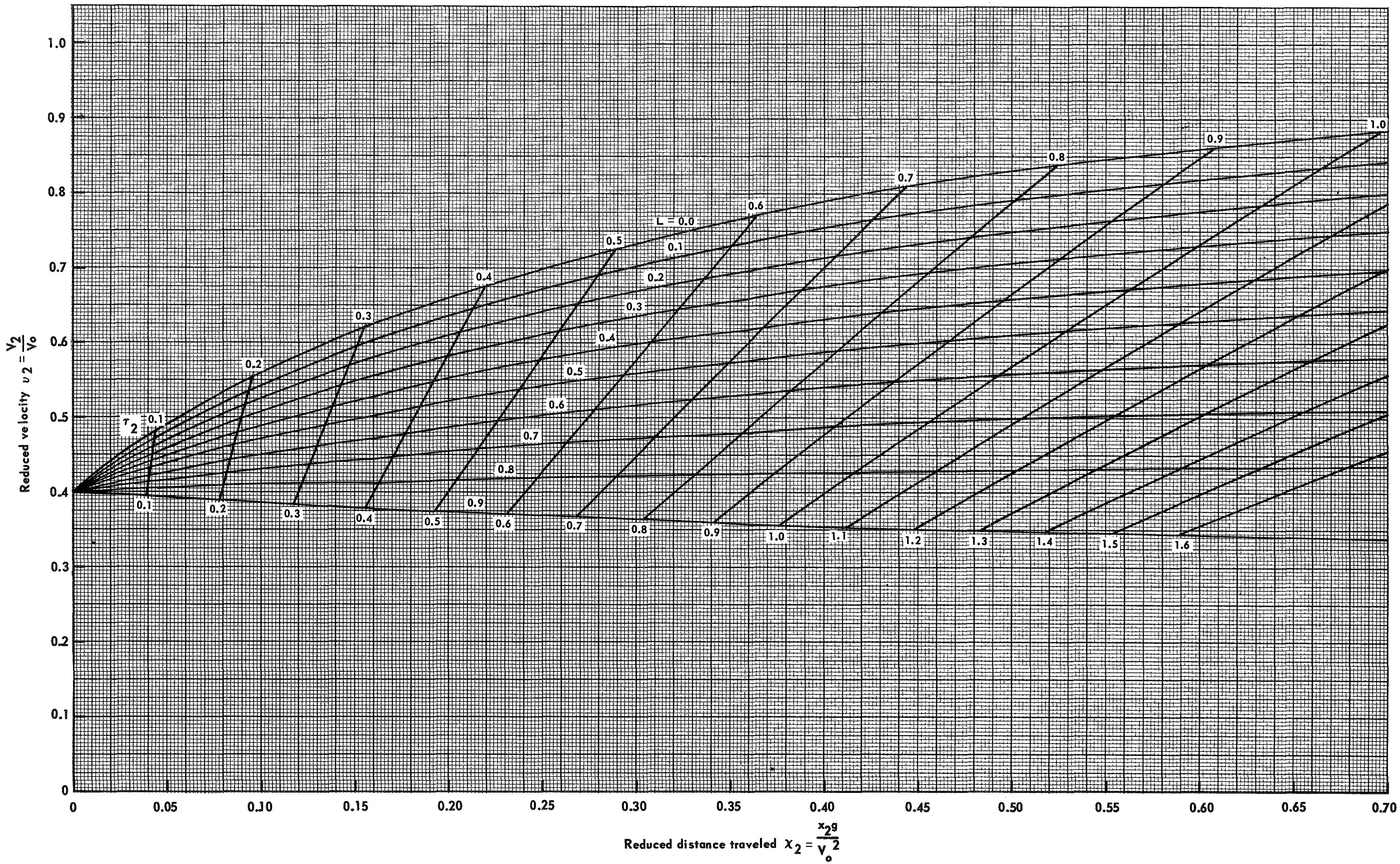

Figure 10 - Dimensionless performance - sustain phase $\upsilon_1 = 0.40$

NASA-S-64-6320

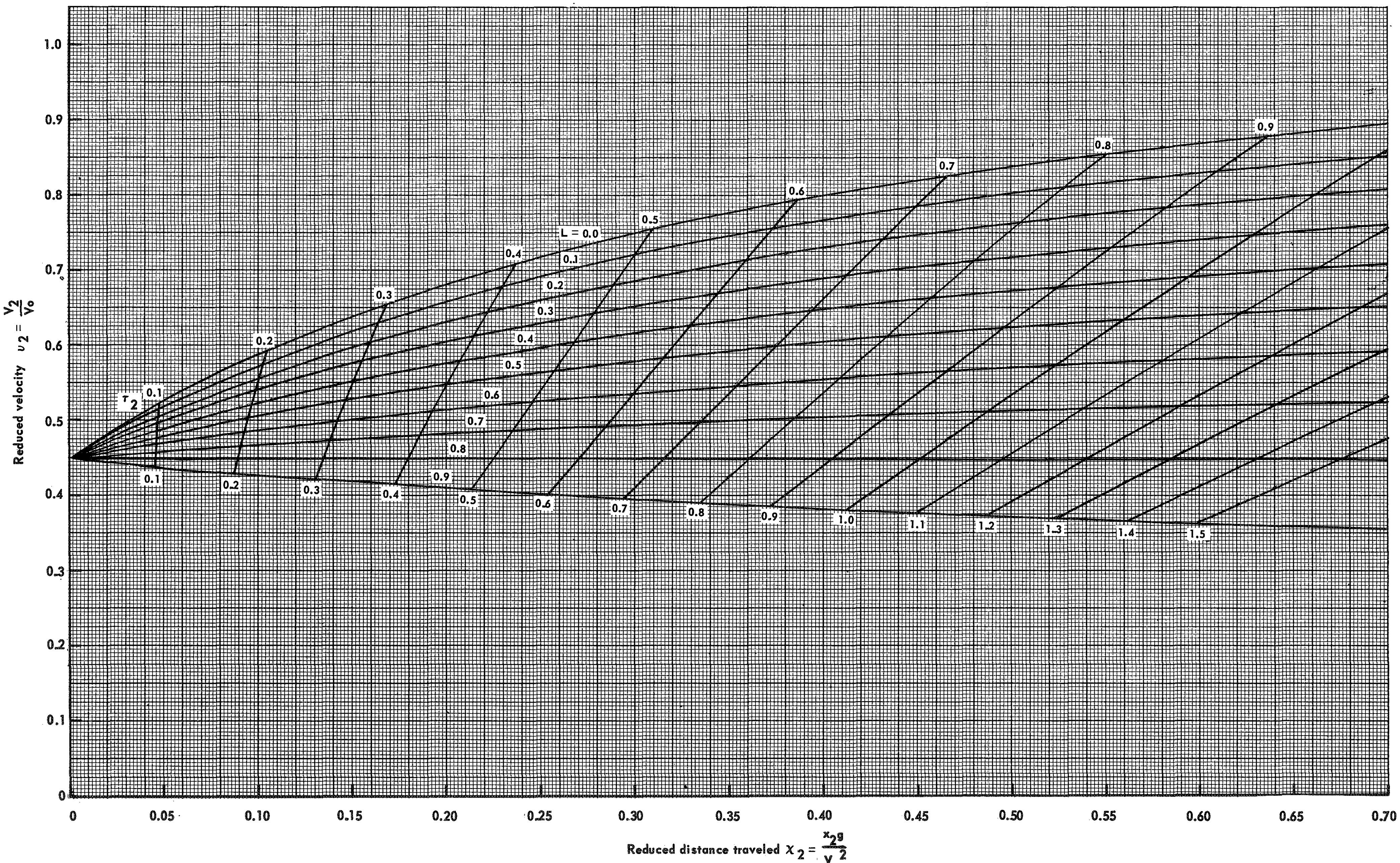

Figure 11 - Dimensionless performance - sustain phase $\upsilon_1 = 0.45$

NASA-S-64-6321

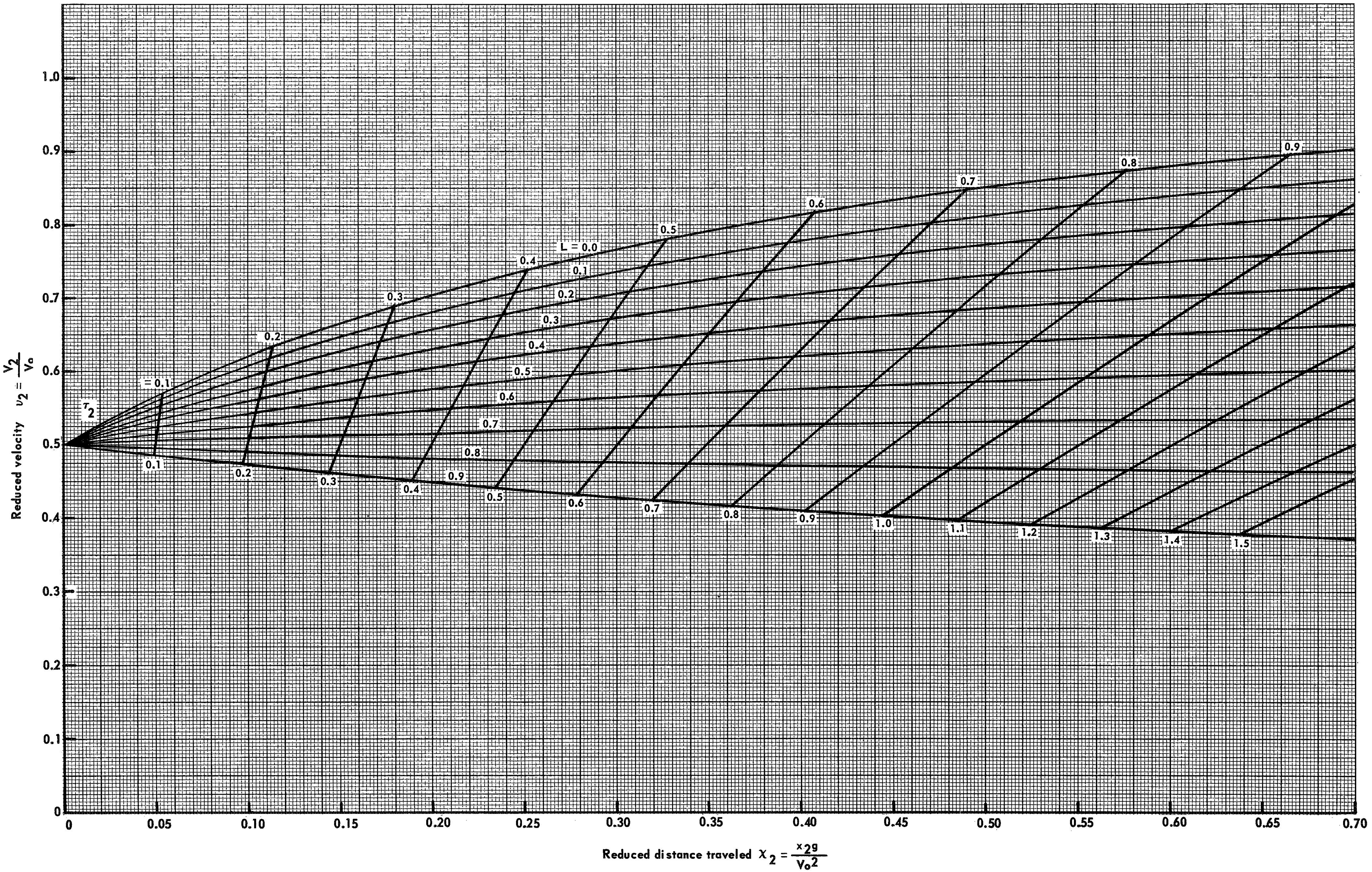

Figure 12 - Dimensionless performance - sustain phase $\upsilon_1 = 0.50$

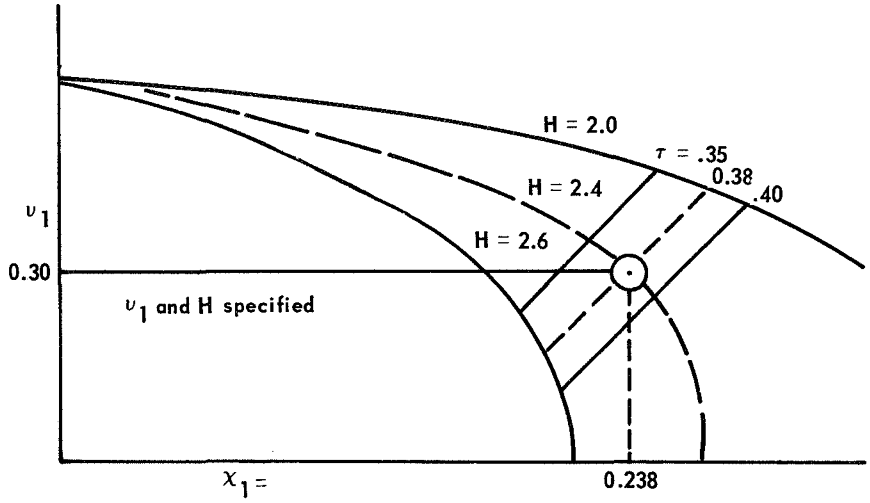

Figure 13 Use of boost phase parametric charts

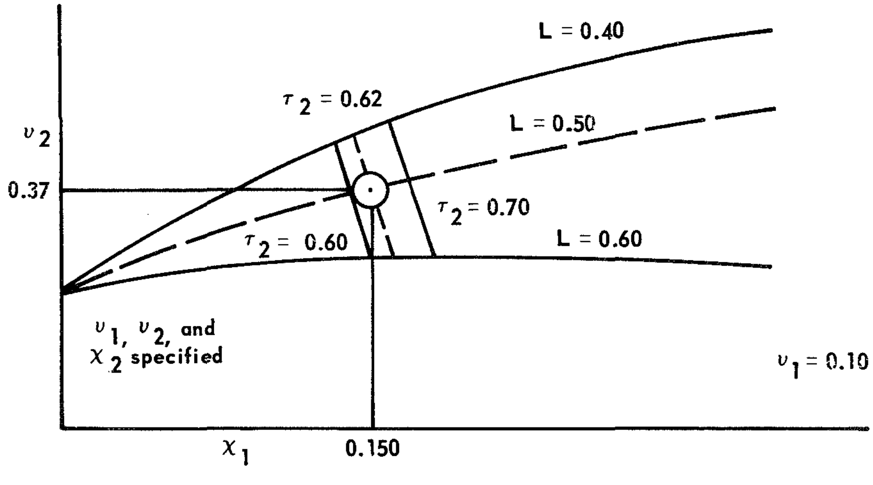

Figure 14 Use of sustain phase parametric chart

NASA-S-64-6324

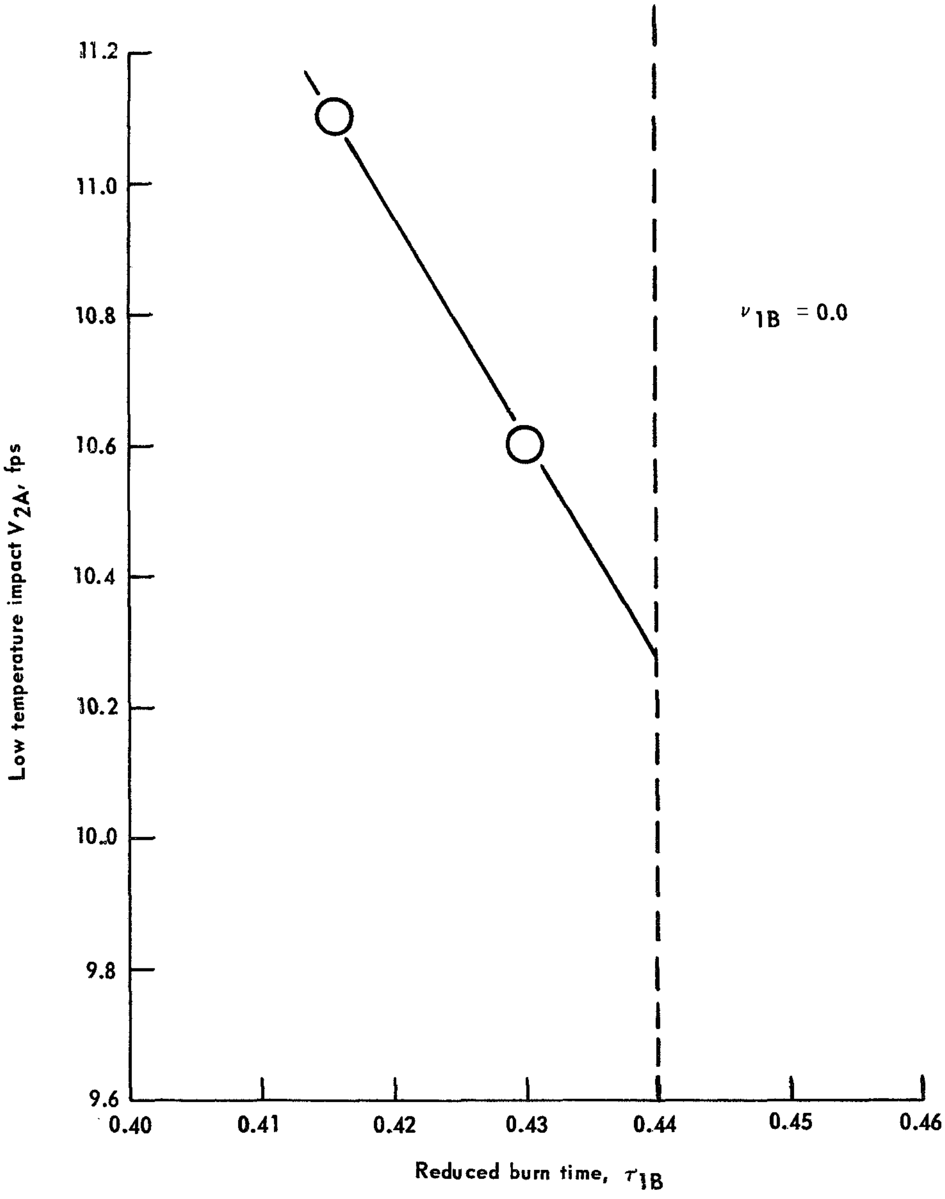

Figure 15 - Illustration of iteration scheme

APPENDIX

PROPULSION MODEL DESCRIPTION AND TESTING

Experimental verification of the above results was required to demonstrate the adequacy of the analytical method. A $\frac{1}{3}$-scale model of the Gemini Spacecraft was chosen as this provided a vehicle of convenient size with which to work. Furthermore, this vehicle was chosen by the Mechanical and Landing Systems Branch (MLSB) of Structures and Mechanics Division (SMD) for subscale tests of the Gemini landing gear. The results of both the propulsion and landing gear tests would be applicable to the Para-Sail landing rocket study.

In order to include the effects of variations of the many parameters affecting system and vehicle performance, a flexible propulsion system was required. Also, the system had to be controllable within close tolerances and safe to operate. A pressurized gas system appeared most likely to meet these requirements; furthermore, it could meet the allowable vehicle weight and volume requirements. The system requirements generated in the main body of this report, scaled down to a 195 lb $\frac{1}{3}$-scale vehicle, are as follows:

	Boost	Sustain
Thrust, lb_f		
Max.	580	110
Nom.	510	100
Min.	470	90
Burning time, sec		
Max.	0.22	0.49
Nom.	0.23	0.51
Min.	0.24	0.53

The schemetic shown in figure A-1 describes the propulsion system selected. The magnitude of the pressure to the nozzle manifold is controlled by the pressure in the dome of the regulator valve. The second, lower pressure level (hence thrust), is achieved by bleeding off some of the dome pressurant.

An electronic control unit was developed by the Guidance and Control Division to control the system's sequence of events. The sequencer used one R-C network channel for opening and closing the regulator dome solenoid valve and one for the nozzle solenoid valve. A start signal was fed into the sequencer by the closing of a microswitch when the model physically separated from the drop tower. This signal initiated both R-C networks; however, both the time to energize and the time to deenergize each circuit were individually controlled by variable potentiometers. These times correspond to the opening and closing signals to each solenoid valve.

In order to effectively use the system, the various operating parameters had to be characterized. Figure A-2 shows the thrust stand used to obtain the relationship between the manifold pressure and the resultant thrust. The propulsion system shown in the figure is not the one described, but that of an earlier configuration. After the tanks were pressurized to approximately 2,500 psi, the regulator was locked open. The nozzle solenoid valve was then opened, allowing the tanks to "blow-down". After replicate runs, the relationship between the resultant thrust and the nozzle manifold pressure, shown in figure A-3, was obtained. The dip in the curve was probably due to flow separation in the nozzle at low manifold pressures.

Before the subsequent steps of characterization, the propulsion system was installed within the framework of the model, as shown in figure A-4. These tests were performed with the vehicle tied down and the nozzles exhausting upward. Arbitrary values of dome solenoid valve and nozzle solenoid valve delay times, d_D and d_N, respectively, and nozzle solenoid valve total time, t_N, were set on the sequencer. A series of tests was made of the propulsion system with various combinations of dome pressure and dome delay times. The dome pressure was varied in steps from 2,000 down to 200 psig. The values of d_D ranged from 620 to 644 msec. Figure A-5 shows the typical relationship found between nozzle manifold and dome pressure, nozzle and dome solenoid valve current values, and time.

Values of nozzle manifold and dome pressure were determined for points 1, 2, 3, and 4 of figure A-5. A summary of these time and pressure relationships is listed in table A-I.

The nozzle manifold pressures at points 2 and 3 were plotted as a function of the dome pressures at points 1 and 4, respectively. This determined the relationship of manifold pressure to the dome pressure, as shown in figure A-6.

The final correlation was obtained by plotting the ratio of dome pressures obtained at points 1 and 4 versus the difference between the sequencer settings t_D and d_D (fig. A-7) or Δt_1.

Since the $\frac{1}{3}$-scale model had negligible drag to help decelerate it, some drag compensation had to be made. The particular approach used was to match the velocity of the model at the end of the boost phase to the calculated velocity at the end of the boost phase if a parachute had been used. This velocity for the full scale vehicle was calculated to be 4.8 fps. The equation for initial velocity for a vehicle acted on by the opposing forces of gravity and constant rocket thrust (no drag) is:

$$V_o = V_1 - (H-1)\, gt_1 \qquad \text{(A-1)}$$

A value of $V_o = 25.5$ fps follows from the results described above for the full scale vehicle, hence 14.7 fps for the $\frac{1}{3}$-scale model.

The scheme for calculating the settings for the sequencer is summarized in table A-II.

The vehicle was placed on the drop rig (fig. A-8), the sequencer settings were made, the tanks pressurized to approximately 3,000 psig, and the dome of the regulator pressurized to the higher value determined in Step II of table A-II. Figures A-9 and A-10 show typical results obtained by the system.

TABLE A-I.- TIME AND PRESSURE RELATIONSHIPS OBTAINED DURING SYSTEM CHARACTERIZATION

Run no.	P_1	P_4	$\frac{P_1}{P_4}$	P_2	P_3	Δt_5	Δt_6	Δt_{11}	d_D	d_N	t_D	t_N	Δt_1
506	2,000	349	5.74	1,410	201	119	92	43	641	326	692	1,242	50
509	1,895	409	4.63	1,360	170	119	93	42	644	328	694	1,244	50
515	1,370	268	5.10	946	170	119	94	43	641	326	691	1,242	50
518	1,580	268	5.90	1,060	161	120	93	41	641	326	697	1,242	56
521	1,149	289	3.97	802	172	121	93	43	636	326	679	1,243	43
527	1,009	329	3.26	700	192	127	94	42	631	326	668	1,245	37
530	809	273	2.97	517	163	126	94	42	633	326	670	1,245	37
533	615	195	3.16	383	115	140	92	46	633	326	669	1,244	36
541	1,520	468	3.25	1,071	144	117	97	49	631	327	667	1,357	36
546	1,763	477	3.67	1,260	135	124	95	40	631	327	671	1,250	40
551	1,580	437	3.70	1,338	292	119	93	42	629	326	669	1,311	40
563	1,792	467	3.65	1,210	321	122	93	42	620	326	660	1,320	40

TABLE A-II. - CALCULATION METHOD FOR SEQUENCER SETTINGS OF COLD GAS SYSTEM

I. Determine high and low manifold pressures from high and low thrust requirements using figure A-3.

II. Determine high and low dome pressures from high and low manifold pressure requirements using figure A-6.

III. Determine the dome pressure vent valve open time, Δt_1, from the ratio of high to low dome pressures using figure A-7.

IV. Calculate the free-fall time required to give the necessary initial velocity from the relationship $t_f = \frac{V_o}{g}$.

V. Calculate the sequencer settings from the following relationships:

$$d_N = t_f - \Delta t_A - \Delta t_5$$

$$t_N = t_f + t_T - \Delta t_6$$

$$d_D = t_f + t_H - \Delta t_{11}$$

$$t_N = d_D + \Delta t_1$$

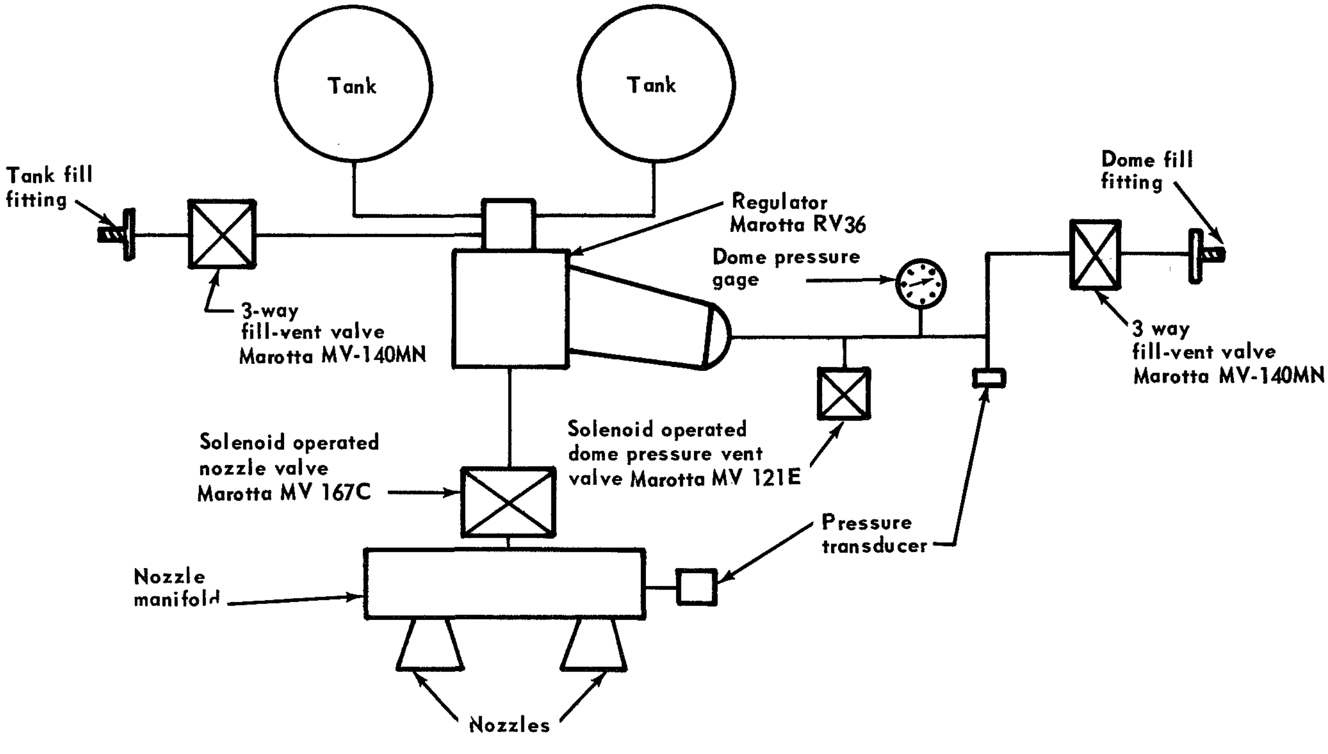
Tank
Tank
Tank fill fitting
3-way fill-vent valve Marotta MV-140MN
Regulator Marotta RV36
Dome pressure gage
Dome fill fitting
3 way fill-vent valve Marotta MV-140MN
Solenoid operated nozzle valve Marotta MV 167C
Solenoid operated dome pressure vent valve Marotta MV 121E
Pressure transducer
Nozzle manifold
Nozzles

Figure A-1 - Schematic of propulsion system (third-scale Gemini)

NASA-S-64-6326

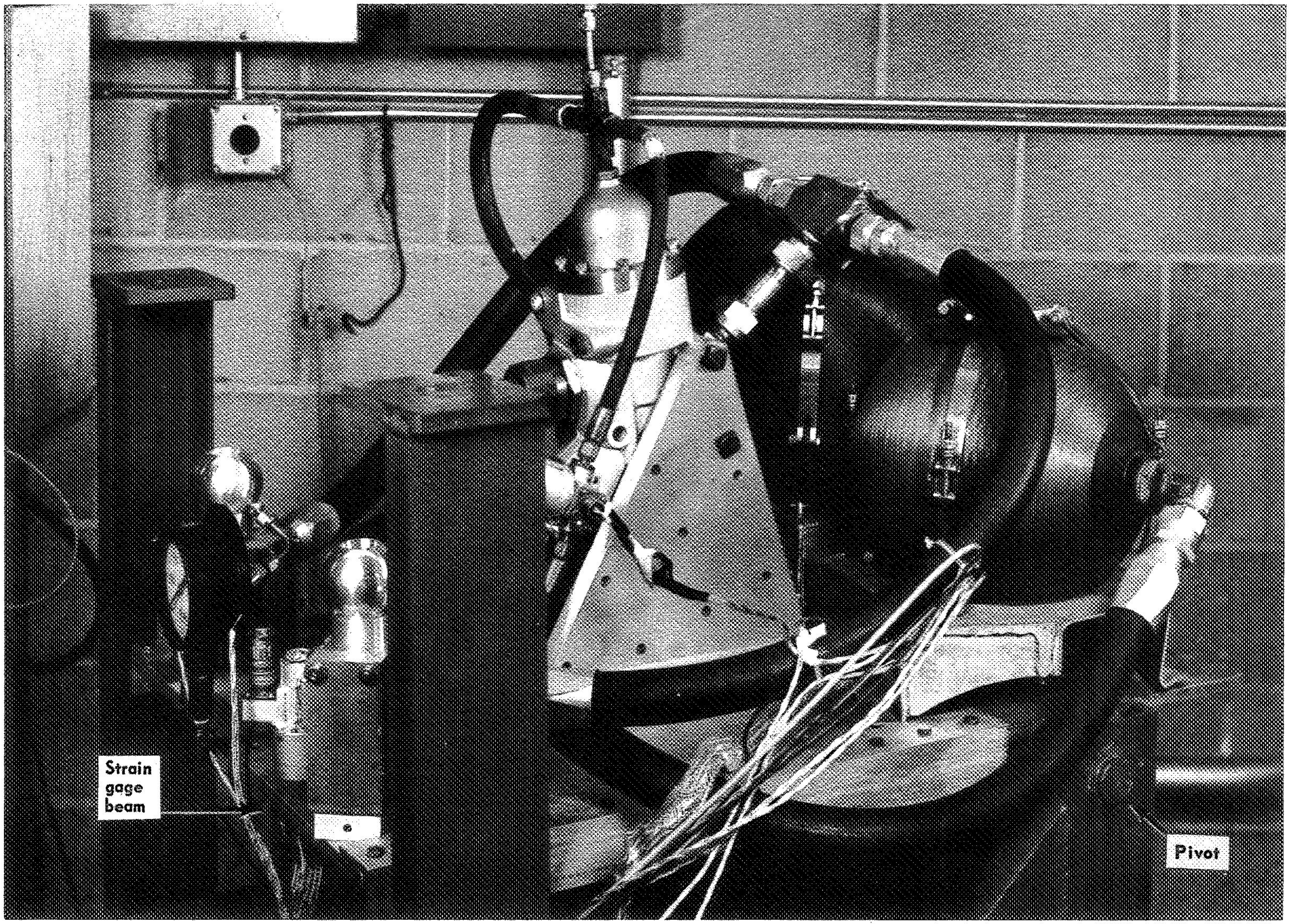
Strain
gage
beam
Pivot

Figure A-2 - Thrust stand used to calibrate cold gas propulsion system

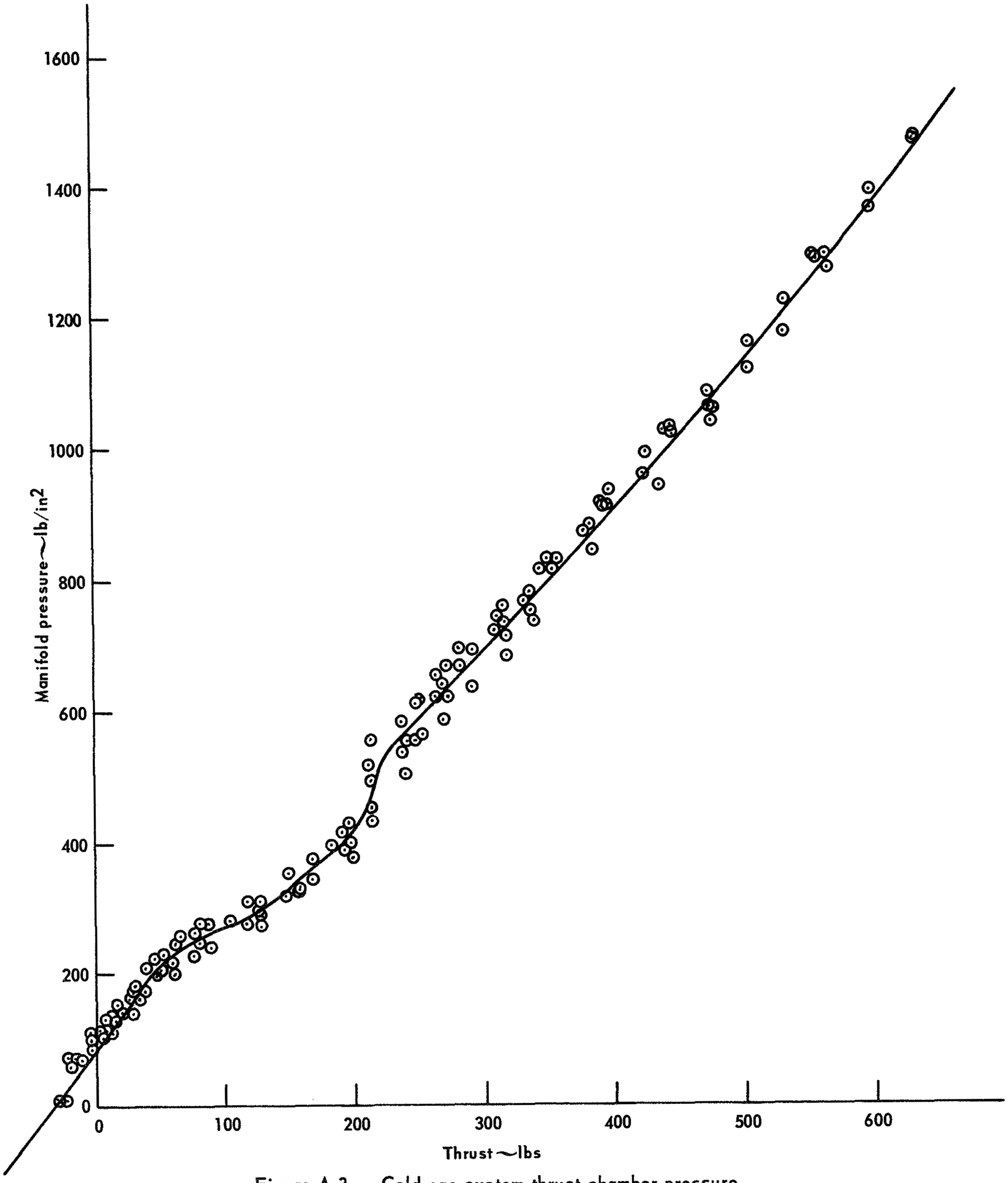

Figure A-3 - Cold gas system thrust-chamber pressure Calibration curve

NASA-S-64-6328

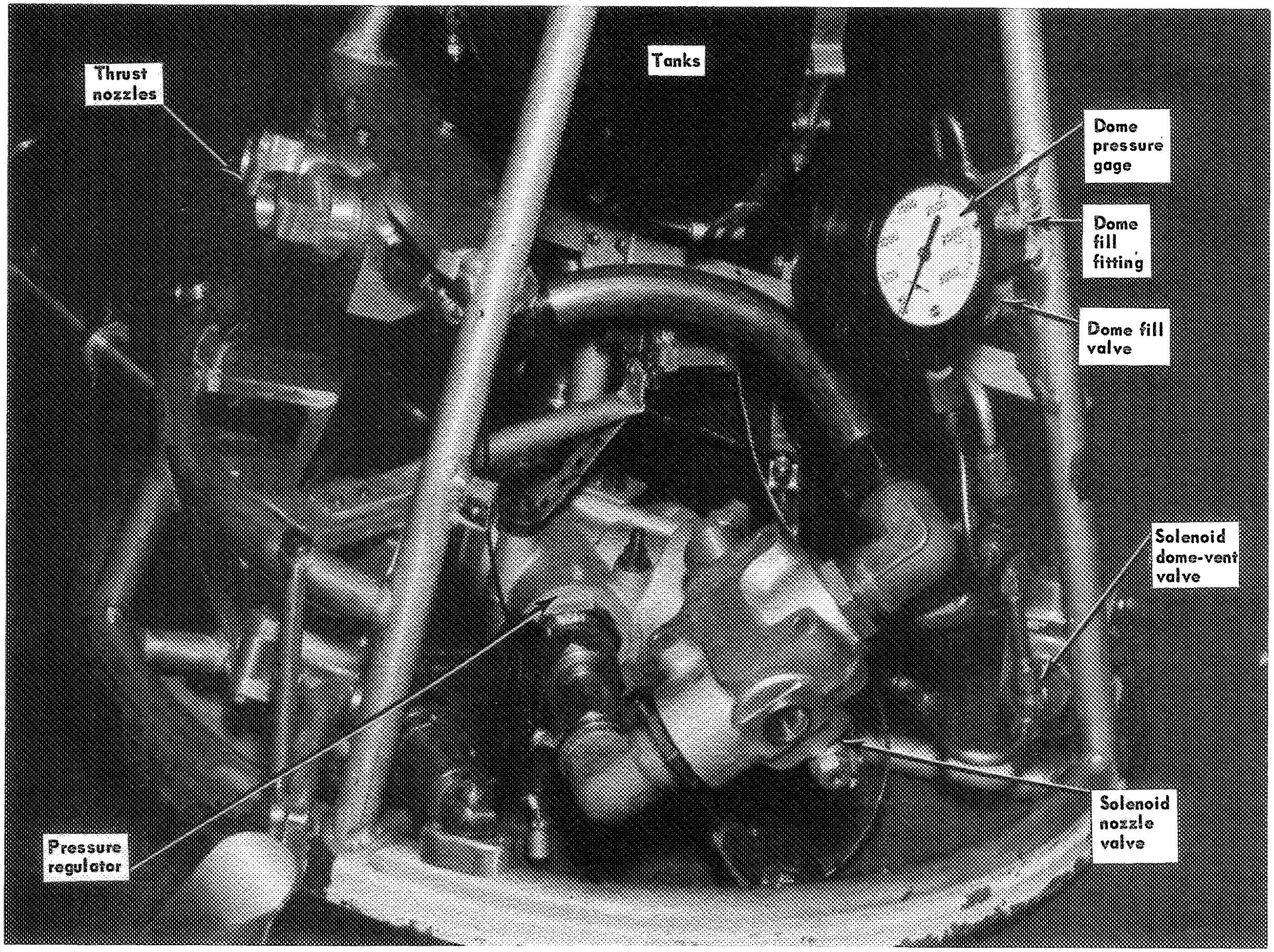
Thrust nozzles
Tanks
Dome pressure gage
Dome fill fitting
Dome fill valve
Solenoid dome-vent valve
Solenoid nozzle valve
Pressure regulator

Figure A-4 - Overall view of model propulsion system

NASA-S-64-6329

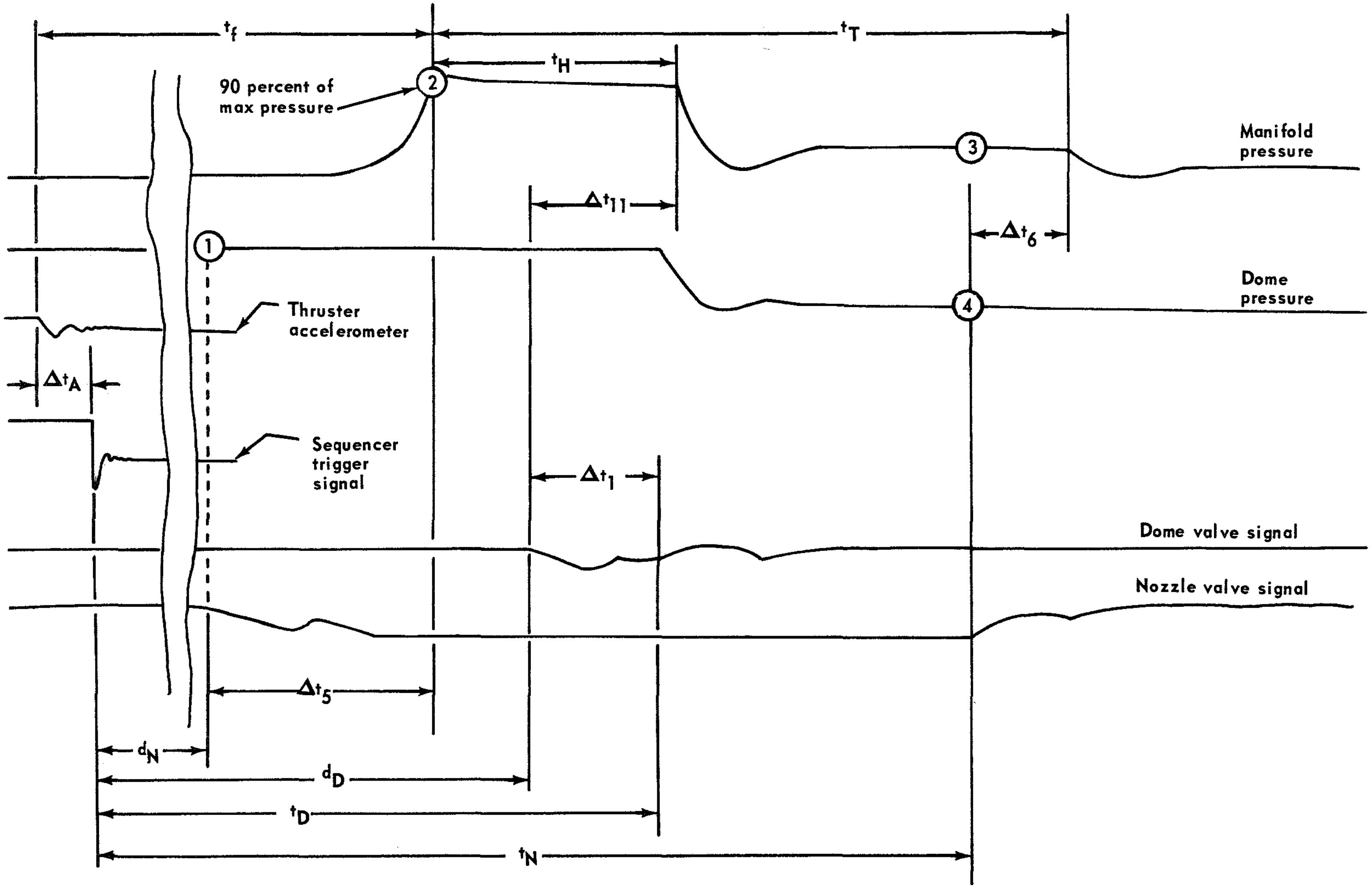
t_f
t_T
t_H
90 percent of max pressure
②
Manifold pressure
③
Δt_{11}
Δt_6
①
Dome pressure
④
Thruster accelerometer
Δt_A
Sequencer trigger signal
Δt_1
Dome valve signal
Nozzle valve signal
Δt_5
d_N
d_D
t_D
t_N

Figure A.5 - Actuation time relationships for cold-gas propulsion system

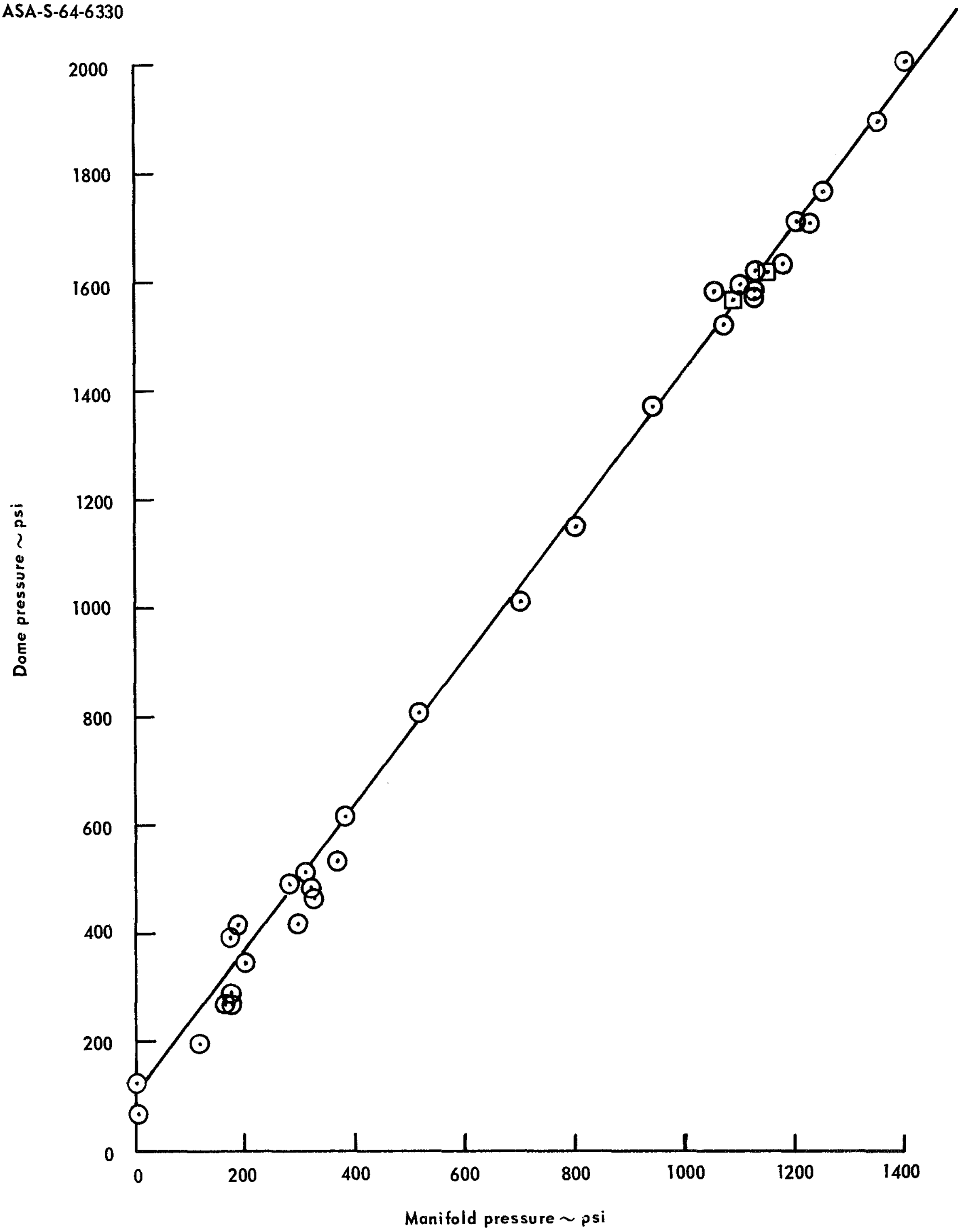

Figure A-6 - Dome pressure-manifold pressure
Calibration curve

NASA-S-64-6331

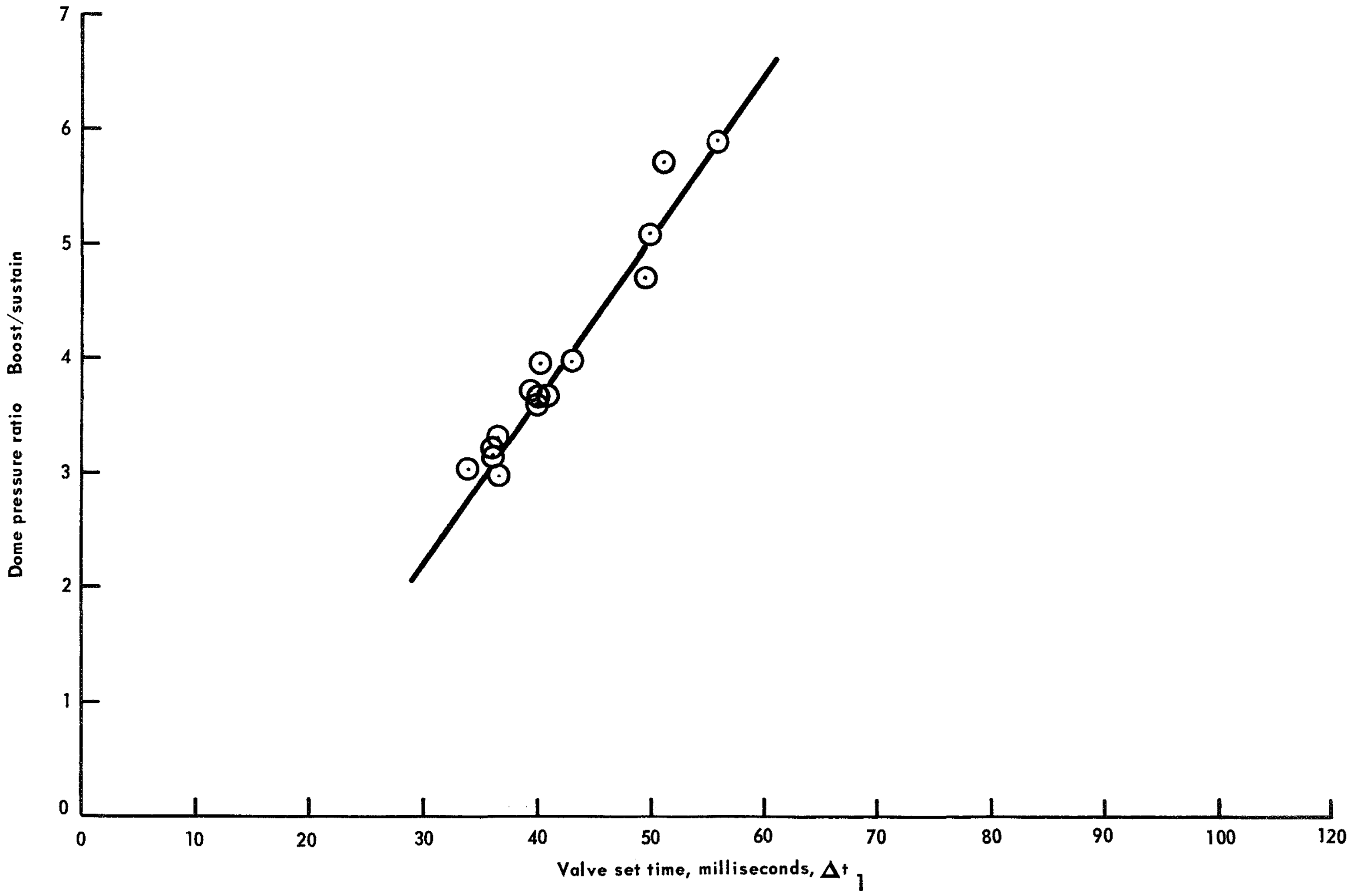

Figure A-7 - Dome pressure ratio as a function of valve open time

NASA-S-64-6332

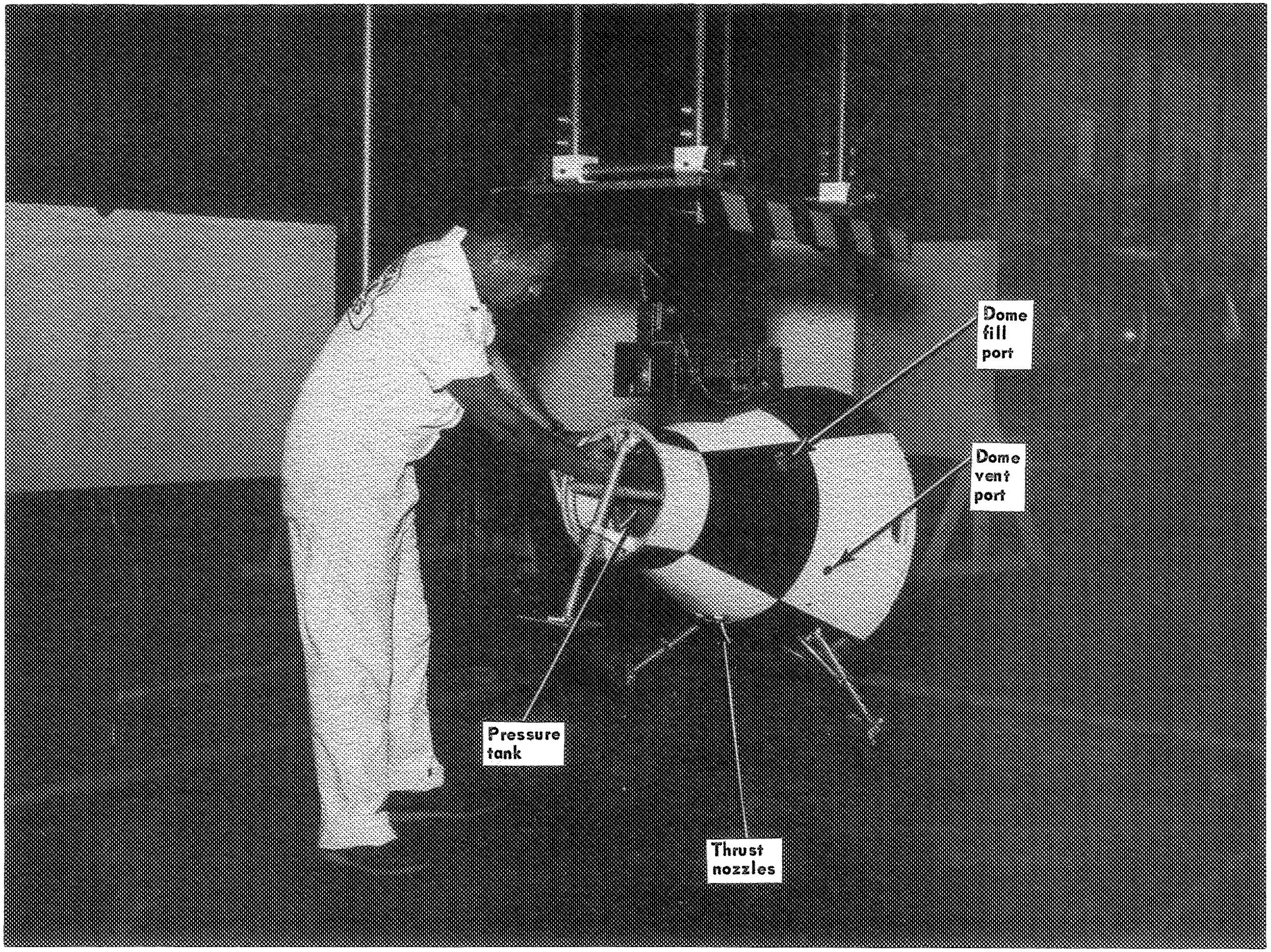
Dome fill port
Dome vent port
Pressure tank
Thrust nozzles

Figure A-8 - Overall model test set-up

NASA-S-64-6333

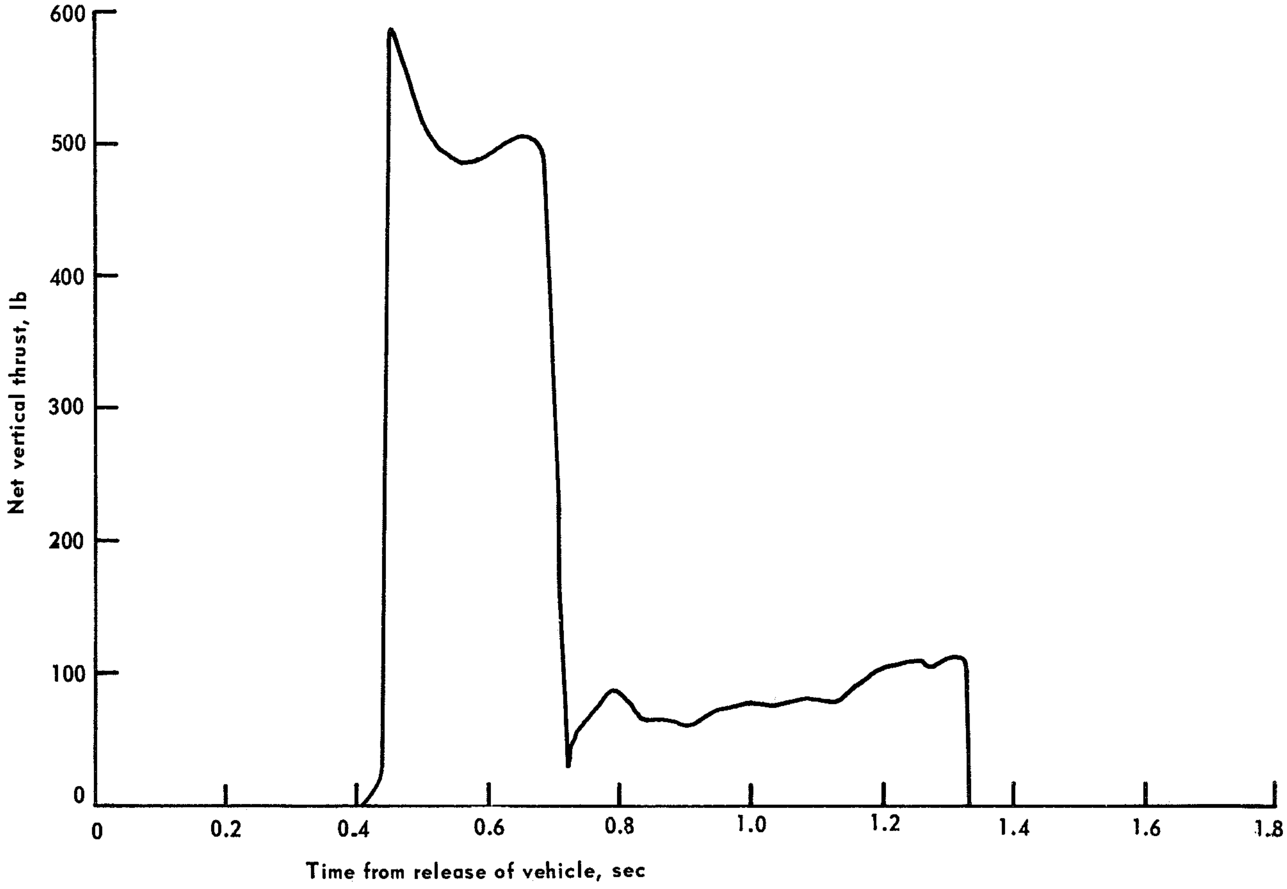

Figure A-9 - Typical cold gas thrust-time variation (drop 25)

NASA-S-64-6334

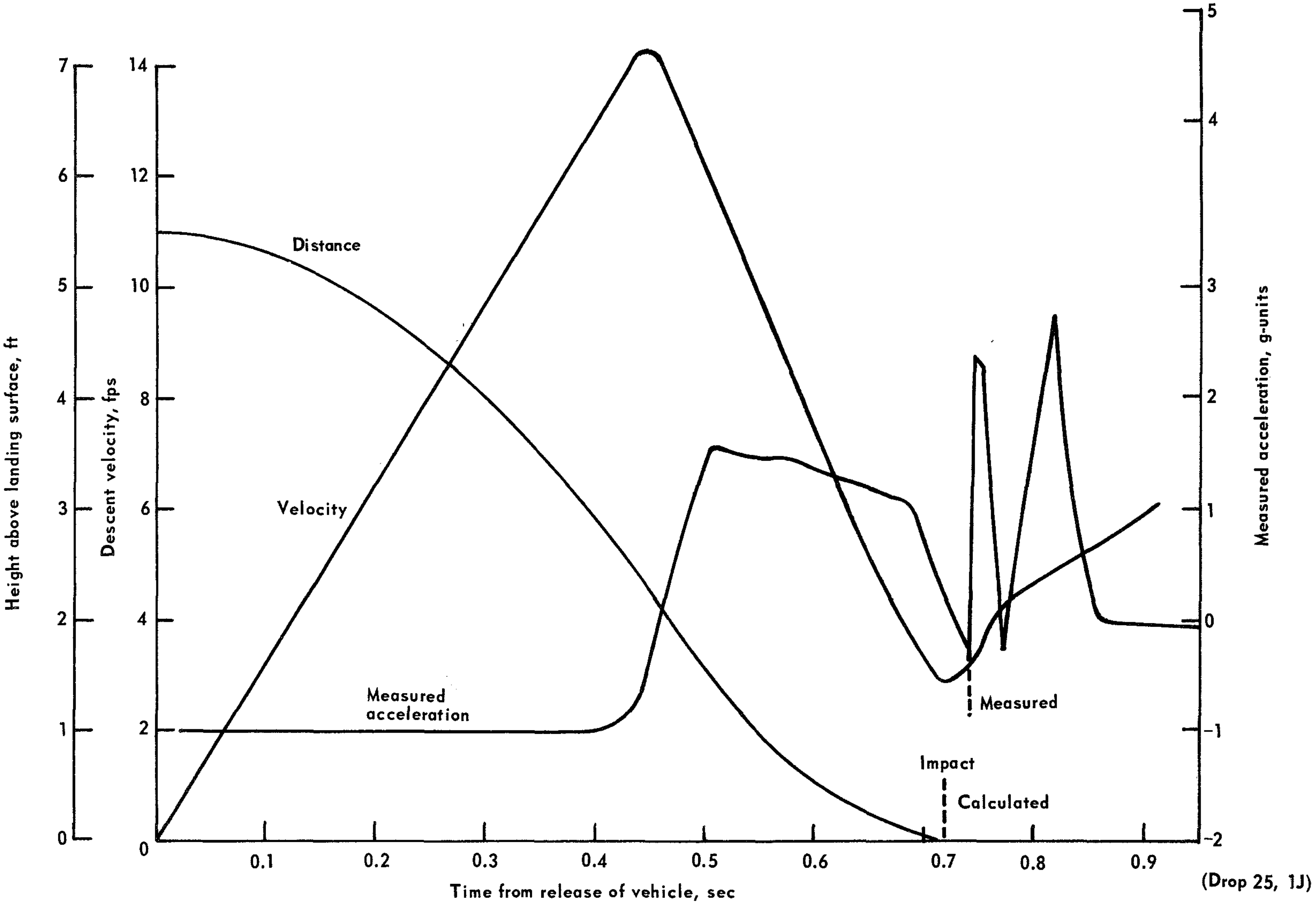

Figure A-10 - Typical vertical acceleration, velocity, distance, and time relationships